Primosomal protein PriC rescues replication initiation stress by bypassing the DnaA-DnaB interaction step for DnaB helicase loading at *oriC*

Ryusei Yoshida, Kazuma Korogi, Qinfei Wu, Shogo Ozaki*, and Tsutomu Katayama*

Department of Molecular Biology, Kyushu University Graduate School of Pharmaceutical Sciences, Fukuoka, Japan
3-1-1 Maidashi, Higashi-ku, Fukuoka 812-8582, Japan

*Corresponding authors: Shogo Ozaki, shogo.ozaki@phar.kyushu-u.ac.jp; Tsutomu Katayama, katayama@phar.kyushu-u.ac.jp

Abstract

In *Escherichia coli*, replisome and replication fork assembly are initiated by DnaB helicase loading at the chromosomal origin *oriC* via its interactions with the DnaA initiator and the DnaC helicase loader. Upon replication fork arrest, the replisome including DnaB dissociates from the stalled fork. Replication fork progression is rescued by primosomal protein PriA- or PriC-dependent pathway in which PriA and PriC promote reloading of DnaB in different mechanisms. However, the mechanism responsible for rescue of blocked replication initiation at *oriC* remains unclear. Here, we found that PriC rescued blocked replication initiation in cells expressing an initiation-specific DnaC mutant, in mutant cells defective in DnaA-DnaB interactions, and in cells containing truncated *oriC* sequence variants. PriC rescued DnaB loading at *oriC* even in the absence of Rep helicase, a stimulator of the PriC-dependent replication fork restart pathway. These and results of *in vitro* reconstituted assays concordantly suggest that this initiation-specific rescue mechanism provides a bypass of the DnaA-DnaB interaction for DnaB loading by PriC-promoted loading of DnaB to the unwound *oriC* region. These findings expand understanding of mechanisms sustaining the robustness of replication initiation and specific roles for PriC in the genome maintenance.

Introduction

Chromosome replication is strictly regulated to ensure successful duplication of the genetic material (Costa & Diffley, 2022; Grimwade & Leonard, 2021; Kasho et al., 2023). In *Escherichia coli*, the ATP-bound form of the replication initiator protein DnaA (ATP-DnaA) forms a higher-order complex with DNA-bending protein IHF at the unique chromosomal origin *oriC*. This complex promotes local unwinding of *oriC* and recruits a pair of DnaB helicases, which are successively loaded to the single-stranded (ss) DNA regions in a bidirectional manner with the aid of DnaC helicase loader.

ssDNA-loaded DnaB interacts with DnaG primase and DNA polymerase III holoenzyme, resulting in replisome (Arias-Palomo et al., 2019; Chodavarapu & Kaguni, 2016; Hayashi et al., 2020; O'Donnell et al., 2013; Sakiyama et al., 2017, 2018, 2022; Wegrzyn & Konieczny, 2023). Replisomes disassemble when the replication fork stalls in front of an obstacle, such as protein-DNA roadblock or single strand breaks. PriA recognizes the abandoned fork structure, which triggers reloading of DnaB with its partner proteins, such as PriB, PriC, DnaT, and DnaC (Heller & Marians, 2005a; Masai et al., 1994; Michel & Sandler, 2017; Windgassen et al., 2018). In addition, independently of PriA, PriC binds to the abandoned fork structure, triggering reloading of DnaB with the aid of DnaC, which is supported by Rep helicase depending on the fork structure (Heller & Marians, 2005b; Sandler et al., 1999). Also, homologous recombination mechanisms can rescue the abandoned replication fork during SOS responses (Asai & Kogomal, 1994; Kogoma, 1997; Né Dicte Michel et al., 2001). In contrast to these well characterized mechanisms at abandoned forks, little is known about what happens when replication initiation is impeded at *oriC*.

E. coli oriC comprises a Duplex-Unwinding Element (DUE) and a DnaA-Oligomerization Region (DOR) (Figure 1A) (Grimwade & Leonard, 2021; Kasho et al., 2023; Wegrzyn & Konieczny, 2023). The DUE contains 13-mer AT-rich sequence repeats known as L-, M-, and R-DUEs. The M- and R-DUEs are essential for stable DUE unwinding with the specific sequences (TT[A/G]T(T)) used for DnaA-ssDNA binding (Ozaki & Katayama, 2012; Sakiyama et al., 2017). The L-DUE containing the TTATT sequence promotes efficient DnaB loading by expanding the unwound *oriC* region (Sakiyama et al., 2022). The DOR is divided into three subregions: the Left-, Middle-, and Right-DORs, which contain asymmetric 9-mer DnaA binding sequences (DnaA box) with the consensus sequence TTA[T/A]NCACA (Figure 1A) (Noguchi et al., 2015; Ozaki & Katayama, 2012; Rozgaja et al., 2011; Sakiyama et al., 2017; Shimizu et al., 2016). The Left-DOR contains a cluster of unidirectionally aligned DnaA boxes including high-affinity DnaA box R1, and low-affinity boxes R5M, τ1−2, and I1-2, with an IHF-binding region between R1 and R5M boxes. The Right-DOR contains an oppositely oriented DnaA box cluster including high-affinity DnaA box R4 and low-affinity boxes I3 and C1-3. These DnaA box clusters form frameworks for the Left- and Right-DnaA subcomplexes, respectively. DnaA bound to the R2 box, which solely resides in the Middle-DOR, stabilizes these DnaA subcomplexes (Miller et al., 2009; Rozgaja et al., 2011; Shimizu et al., 2016). In addition, the AT-cluster (TATTAAAAAGAA) region, which connects to the L-DUE, stimulates DnaB loading in the absence of the Right-DnaA subcomplex (Sakiyama et al., 2022).

DnaA comprises four functional domains (Figure 1B). Domain I binds to multiple proteins such as DnaB helicases and the DnaA-assembly stimulator DiaA (Abe et al., 2007; Hayashi et al., 2020; Keyamura et al., 2007, 2009). Domain II is a flexible linker (Abe et al., 2007; Nozaki & Ogawa, 2008).

Domain III contains AAA+ (ATPases Associated with various cellular Activities) motifs, which are involved in tight ATP/ADP binding, ATP hydrolysis, and domain III-III interactions (Duderstadt et al., 2011; Erzberger et al., 2006; Felczak & Kaguni, 2004; Kawakami et al., 2005; Ozaki et al., 2012). The arginine finger motif (Arg285) in domain III interacts with ATP bound to domain III of adjacent DnaA protomers, stimulating DnaA complex formation in a cooperative manner (Kawakami et al., 2005; Noguchi et al., 2015). In addition, H/B motifs (Val 211 and Arg245) in this domain bind to ssDNA in a sequence-specific manner (Ozaki et al., 2008; Sakiyama et al., 2017). Domain IV, which comprises the helix-turn-helix motif, recognizes the DnaA box (Fujikawa et al., 2003).

For replication initiation, ATP-DnaA molecules cooperatively oligomerize at *oriC* to form the Left- and Right-DnaA subcomplexes (Figure 1C). Formation of these complexes is stimulated by homotetrameric DiaA protein, which binds up to four DnaA molecules via domain I, including Phe46 (Keyamura et al., 2007, 2009). In concert with DNA superhelicity and thermal energy, the DUE undergoes initial unstable unwinding, which is stabilized through specific interaction between H/B motifs of domain III in the Left-DnaA subcomplex and the upper strand of M- and R-DUEs. This interaction is facilitated by sharp DNA bending by IHF, resulting in stable DUE unwinding (Figure 1C) (Ozaki et al., 2008; Sakiyama et al., 2017). When the single-stranded region is expanded to the L-DUE, the resultant single-stranded L-DUE binds the H/B motifs within the Right-DnaA subcomplex, maximizing the efficiency of the DnaB loading process (Sakiyama et al., 2022).

Subsequently, two DnaB helicases are loaded onto each ssDUE strand through interactions with DnaC and DnaA (Figure 1D). DnaC binding to DnaB changes the closed ring structure of the DnaB hexamer to an open spiral form to allow it to encircle ssDNA (Arias-Palomo et al., 2019; Nagata et al., 2020). Each Left- and Right-DnaA subcomplex binds a DnaB-DnaC complex via high-affinity interaction between DnaA Phe46 and DnaB Leu160 and guides the DnaB-DnaC complexes to unwound ssDUE strands via a low-affinity interaction between DnaA domain III His136 and DnaB (Figure 1B and 1D). Upon interaction with ssDNA, DnaC dissociates from DnaB, which enables migration of DnaB hexamer with helicase action. The pair of DnaB helicases loaded onto the ssDNA strands progress in opposite directions, forming replisomes with DnaG and Pol III holoenzyme (Chodavarapu & Kaguni, 2016; O'Donnell et al., 2013).

Replication restart pathways ensure fork progression of the entire chromosome under conditions that trigger replisome disassembly (Heller & Marians, 2005a; Lopper et al., 2007; Michel & Sandler, 2017). PriA helicase-dependent pathways predominantly facilitate DnaB reloading onto abandoned forks *in vivo* (Flores et al., 2002). PriA is a 3'-5' DNA helicase and has specific affinity for forked DNA structures comprising one parental dsDNA and two newly synthesized sister dsDNA strands. This permits PriA recognition of the abandoned replication fork and the subsequent unwinding of the nascent lagging

strand (Duckworth et al., 2023; Windgassen et al., 2018; Windgassen & Keck, 2016). The resultant unwound ssDNA associates with PriB and DnaT to promote reloading of DnaB helicase with the aid of DnaC (Duckworth et al., 2023; Heller & Marians, 2005a; Lopper et al., 2007). In the absence of PriB, PriC participates in a PriA-dependent pathway (Sandler et al., 1999). In addition, PriA is required for *oriC*/DnaA-independent chromosomal replication called stable DNA replication (SDR) (Masai et al., 1994), which is promoted by UV irradiation (inducible iSDR) and loss of *rnhA* or *recG* (constitutive cSDR) (Kogoma, 1997). In both mechanisms, replication is initiated at triple-stranded structures comprising a dsDNA-ssDNA hybrid (D-loop) or a dsDNA-ssRNA hybrid (R-loop) generated at specific chromosomal loci. These structures mimic the abandoned fork structure, thereby allowing helicase loading to occur similarly to that during PriA-dependent fork restart (Masai et al., 1994).

Independently of PriA, PriC can restart replication from abandoned forks through its interaction with the ssDNA region and SSB (Single-Stranded DNA Binding protein) (Figure 1E) (Heller & Marians, 2005a; Wessel et al., 2013, 2016). PriC consists of N-terminal and C-terminal domains, which are composed of α helices and are connected by a short linker. The PriC C-terminal domain remodels the SSB-ssDNA complex, which is a prerequisite for the recruitment of DnaB helicase (Heller & Marians, 2005a; Wessel et al., 2013, 2016). PriC also interacts with Rep helicase. When the length of the ssDNA gap within the abandoned fork is short, Rep helps expand the ssDNA gap, promoting PriC-mediated remodeling of the SSB-ssDNA complex (Heller & Marians, 2005a, 2005b; Nguyen et al., 2021). Notably, in addition to these functions at the abandoned forks, PriC is suggested to play a role in DnaA-*oriC*-dependent replication initiation under challenging conditions, as evidenced by the synthetic lethality between *priC303*::*kan* and a subgroup of temperature-sensitive *dnaA* mutant alleles (*dnaA46* and *dnaA508*): i.e. *priC303*::*kan* mutants bearing *dnaA46* or *dnaA508*, but not wild-type (WT) *dnaA*, can not grow even at 30°C (Hinds & Sandler, 2004). However, the mechanisms via which PriC rescues blocked replication initiation remain elusive.

In this study, we analyzed the PriC-dependent promotion of replication initiation from *oriC* in the context of various replication initiation stresses. We found that PriC stimulated replication initiation in *dnaC2* cells, in which DnaB helicase loading at *oriC* is defective, indicating that it has a role in the rescue of blocked replication initiation. Moreover, PriC stimulated the growth of cells defective in DnaA-DnaB interactions in addition to the growth of cells with *oriC* sequence deletions that inhibit DnaB loading. Consistent with these results, in an *in vitro* reconstituted system, PriC stimulated DnaB loading when the DnaA-DnaB interaction was inhibited at *oriC*. Furthermore, we found that PriC did not stimulate initiation of cSDR, demonstrating that PriC functions specificity in the DnaA-*oriC* system. Taken together, we suggest that PriC rescues blocks in replication initiation by bypassing DnaB loading by *oriC*-DnaA complexes.

140

141 **Results**

142 **PriC stimulates DNA replication initiation in *dnaA46* and *dnaC2* cells.**

143 The temperature-sensitive *dnaA46* and *dnaA508* mutants exhibit synthetic lethality with
144 *priC303*::*kan* even at 30°C (Hinds & Sandler, 2004), suggesting that PriC can rescue blocks in DnaA-
145 dependent replication initiation. However, the mechanism underlying PriC-promoted rescue of blocks in
146 replication initiation remains a mystery. Based on previous reports demonstrating PriC binding to short
147 oligo-ssDNA, SSB, and DnaB and its role in DnaB loading at stalled replication forks (Wessel et al., 2013,
148 2016), we considered the possibility that PriC permits bypass of DnaA-dependent stable DUE unwinding
149 and/or DnaB loading at the *oriC* ssDUE. To genetically test these ideas, we analyzed the impact of PriC
150 on the growth of a temperature-sensitive *dnaC2* mutant, which is competent for ongoing replisome
151 progression at 37–42°C, but defective in DnaB loading specifically at the *oriC* ssDUE (Withers &
152 Bernander, 1998).

153 Colony formation of *dnaA46* cells was moderately inhibited at 37°C (Figure 2A). Consistent
154 with a previous report, when crossed with the Δ*priC* allele, colony formation of *dnaA46* mutant cells
155 but not WT *dnaA* cells was severely inhibited at 37°C (Figure 2A). Unlike the *dnaA46 priC303*::*kan*
156 mutant, *dnaA46* Δ*priC* cells formed colonies at 30°C, although colony growth was slightly retarded.
157 This difference may stem from the different strain backgrounds. Notably, colony formation of *dnaC2*
158 cells at 35°C was moderately inhibited, whereas it was severely inhibited in *dnaC2* Δ*priC* cells (Figure
159 2A). At 30°C, colony formation by *dnaC2* cells and *dnaC2* Δ*priC* cells was similar. The observed
160 requirement for PriC for colony formation by *dnaC2* cells at 35°C supports the idea that PriC assists in
161 the DnaC-dependent DnaB loading step at *oriC*.

162 To investigate replication initiation from *oriC*, we used flow cytometry of synchronized cells
163 bearing *dnaA46* or *dnaC2* with or without Δ*priC*. In these experiments, cells were incubated at 42°C or
164 37°C for 80–90 min to synchronize the replication cycle at the pre-initiation step, after which
165 incubation was continued at 30°C for 5 min to allow initiation and then 4 h in the presence of
166 rifampicin and cephalexin to inhibit both replication initiation and cell division and allow replication
167 run-out of the whole chromosome. The resultant number of chromosomes per cell, measured by flow
168 cytometry, is known to correspond to the number of *oriC* copies per cell at the time of drug addition, an
169 indicator of initiation activity.

170 A majority of the synchronized *dnaA46* and *dnaC2* cells had only a single *oriC* copy per cell
171 after incubation at 42°C or 37°C regardless of the presence of Δ*priC* (Figure 2B and 2C). In WT *priC*
172 cells, after release of initiation at 30°C for 5 min, most cells had two *oriC* copies. However, in *dnaA46*
173 Δ*priC* cells, only about half of the cells had two *oriC* copies after the release (Figure 2B), indicating

174 moderate inhibition of initiation. In *dnaC2* Δ*priC* cells, the number of two-*oriC* cells was slightly lower
175 than that of *dnaC2* cells (Figure 2C). These observations are consistent with the colony formation data
176 and with our hypothesis that PriC contributes to the rescue of blocked replication initiation by assisting
177 DnaB loading onto the *oriC* ssDNA.
178
179 **PriC rescues the cell growth of DnaA mutants defective in DnaB interactions.**
180 DnaA contains two regions for interactions with DnaB during DnaB loading at *oriC* ssDNA:
181 one is a high-affinity region in domain I containing Phe46, and the other is a low-affinity region in
182 domain III containing His136. To analyze the mechanism of PriC-promoted DnaB loading at *oriC*, we
183 introduced a series of pING1 vector-based plasmids encoding WT DnaA (pKA234) or the DnaA F46A
184 H136A double mutant (pFH) into *dnaA46* cells with or without WT *priC*. Growth of *dnaA46* cells
185 containing pING1 was inhibited at 42°C, but the leaky expression of *dnaA* from pKA234 enabled the
186 growth of these cells, as previously reported (Sakiyama et al., 2018) (Figure 3). Introduction of pFH
187 moderately supported colony formation by *dnaA46* cells at 42°C. By contrast, *dnaA46* Δ*priC* cells
188 carrying pFH exhibited little growth at 42°C (Figure 3). These results suggest that PriC is crucial for the
189 growth of cells defective in specific DnaA-DnaB interactions, possibly because it can bypass the DnaA-
190 DnaB interaction step required for DnaB loading onto *oriC* ssDNA.
191
192 **PriC rescues DNA replication inhibition by DiaA overexpression *in vivo*.**
193 DiaA, a homotetrameric protein, binds to multiple DnaA molecules and stimulates DnaA
194 multimer assembly at *oriC* (Keyamura et al., 2007). The Phe46 residue in DnaA domain I is part of the
195 DiaA-binding site and DnaB binding site. Oversupply of DiaA inhibits timely initiation of replication in
196 cells growing in tryptone medium at 30°C, probably because of binding competition between DiaA and
197 DnaB for DnaA domain I (Ishida et al., 2004; Keyamura et al., 2009). If PriC can bypass the DnaA-
198 DnaB interaction requirement for DnaB loading onto *oriC*, PriC should suppress inhibition of initiation
199 by DiaA oversupply. To test this possibility, we introduced pBR322 or its derivative encoding *diaA*
200 (pNA135) into cells with or without WT *priC* (Figure 4). WT *priC* cells carrying pBR322 or pNA135
201 similarly formed colonies on LB agar plates containing ampicillin between 25°C and 42°C (Figure 4A
202 and Figure 4-figure supplement 1). However, in Δ*priC* cells carrying pNA135, but not pBR322, colony
203 formation was moderately inhibited at 25°C (Figure 4A), supporting our conjecture that PriC can
204 bypass the requirement for the DnaA-DnaB interaction.
205 Rep helicase stimulates PriC-mediated rescue of arrested replication forks containing nascent
206 strands (Heller & Marians, 2005b, 2005a; Sandler, 2000). To test the contribution of Rep helicase to

207 PriC-promoted rescue of blocked replication initiation, we introduced pBR322 or pNA135 into Δ*rep*
208 cells. Unlike Δ*priC* cells, Δ*rep* cells carrying pNA135 grew similarly to Δ*rep* cells carrying pBR322
209 (Figure 4A), suggesting no involvement of Rep in the PriC-promoted rescue of blocked replication
210 initiation. This is consistent with the features of unwound *oriC*, which has a fork structure similar to
211 that of the replication fork but without nascent strands, and the specific role of Rep in rescuing
212 abandoned replication forks with nascent strands in the PriC-dependent pathway. Rep is specifically
213 required for the unwinding of the nascent leading strand of abandoned replication forks, which is
214 needed to expand the ssDNA region required for entry of PriC (Heller & Marians, 2005b, 2005a).
215 We further analyzed replication initiation in Δ*priC* cells carrying pNA135 at 30°C by flow
216 cytometry (Figure 4B). Exponentially growing cells were further incubated for run-out replication after
217 the addition of rifampicin and cefalexin. The volume (mass) of cells at the time of drug addition was
218 also quantified. Under these conditions, WT *priC* cells bearing pBR322 mainly had eight or four *oriC*
219 copies per cell with eight-*oriC* cells predominating (Figure 4B). The number of *oriC* copies per cell was
220 similar to that in WT *priC* cells bearing pNA135, with only slight increase of asynchronous initiation,
221 as shown by the slight increase in the number of cells with non-2^n *oriC* copies, which is basically
222 consistent with our previous data (Ishida et al., 2004). However, in Δ*priC* cells bearing pNA135, severe
223 inhibition of initiation occurred, as shown by the substantial decrease in the number of eight-*oriC* cells
224 and the large increase of the number of cells with only one to three *oriC* copies (Figure 4B). This result
225 supports the proposed function of PriC at *oriC* mentioned above. In addition, the observed
226 asynchronous initiations in Δ*priC* cells bearing pBR322 is worthy of attention. Indeed, the fraction of
227 cells with non-2^n *oriC* copies was higher among Δ*priC* cells than among WT *priC* cells (Figure 4B),
228 suggesting that even in normal cells, inhibition of replication initiation occurs at low frequency and
229 requires PriC function to rescue replication initiation.
230 To test whether PriC rescues replication initiation inhibited by deletion of the *diaA* gene, we
231 conducted similar flow cytometry analysis of Δ*priC*, Δ*diaA*, and Δ*priC* Δ*diaA* cells (Figure 4C). Δ*diaA*
232 cells showed severe asynchrony of replication initiation, as shown by the increase in the number of five-
233 to-seven-*oriC* cells, which supports the stimulatory role of DiaA in DnaA-*oriC* complex formation
234 (Figure 4C). However, Δ*priC* Δ*diaA* cells did not show more asynchronization of replication initiation
235 than Δ*diaA* cells, as shown by the similar asynchrony index (A.I.). These results suggest that PriC does
236 not support or bypass DnaA-*oriC* complex formation.
237
238 **PriC stimulates replication initiation in cells with *oriC* sequence truncations**
239 Right DnaA-subcomplex plays a stimulatory role in DnaB helicase loading (Sakiyama et al.,
240 2022). The loading of two DnaB hexamers at *oriC* ssDNA regions requires multiple steps that depend

241 on the distinct functions of two DnaA subcomplexes (Figure 1): the Left-DnaA subcomplex stably
242 unwinds M-R regions of the DUE and the Right-DnaA subcomplex expands the unwound region to the
243 AT-L region, supporting efficient DnaB helicase loading (Sakiyama et al., 2017, 2022; Yoshida et al.,
244 2023). The expanded ssDNA regions in this open *oriC* complex efficiently promote the loading of one
245 DnaB hexamer onto the lower (A-rich) strand M-R region and a second DnaB hexamer onto the upper
246 (T-rich) strand of the DUE (Fang et al., 1999; Sakiyama et al., 2022). In the absence of the Right-DnaA
247 subcomplex, the AT region of the AT-L region assists in DnaB loading (Sakiyama et al., 2022;
248 Stepankiw et al., 2009)

249 To determine whether PriC rescues defects in DnaB loading when the *oriC* sequence is altered
250 to prevent Right-DnaA subcomplex formation, we first assessed the colony formation of cells lacking
251 the Middle- and Right-DOR of *oriC* (Left-*oriC*) (Figure 5A). The Left-*oriC* mutant formed colonies at
252 37°C but showed severe growth defects at 25°C and 30°C (Figure 5B). At 37°C, thermal energy might
253 be sufficient to expand DUE unwinding into the AT region and allow DnaB loading in the absence of
254 the Right-DnaA subcomplex (Sakiyama et al., 2022), but not at 25°C or 30°C. By contrast, colony
255 formation of the Left-*oriC* Δ*priC* double mutant was markedly compromised at 37˚C (Figure 5B) and
256 the growth defects of the Left-*oriC* mutant 25°C and 30°C were aggravated. These findings support the
257 idea that PriC functions to rescue defective processes in DnaB loading caused by deletions of the *oriC*
258 sequence that prevent DnaA subcomplex formation.

259 Next, similar experiments were performed using a mutant in which the R4 DnaA box within
260 Right-DOR was substituted with a sequence (R4*Tma*) defective in binding of *E. coli* DnaA (Figure 5A
261 and 5C) (Noguchi et al., 2015; Sakiyama et al., 2022). We reasoned that formation of the Right-DnaA
262 subcomplex would be inhibited by the introduction of R4*Tma* and PriC would be required for robust
263 initiation in this context. As in the Left-*oriC* strain, the R4*Tma* strain showed normal colony formation
264 in the presence of WT *priC*. By contrast, in the R4*Tma* Δ*priC* strain, colony formation was impaired
265 moderately at 25°C and slightly at 30°C (Figure 5C), indicating that PriC can rescue the blocked
266 replication initiation caused by the absence of the R4 box. The reduced colony formation of R4*Tma*
267 Δ*priC* double mutant cells was alleviated at higher temperatures, similar to the phenotype of the Left-
268 *oriC* mutant.

269 Furthermore, we assessed replication initiation in R4*Tma* cells at 30°C using flow cytometry
270 (Figure 5D). R4*Tma* cells grew slightly slower than WT *oriC* cells and showed clear inhibition of
271 initiation; in contrast to the WT *oriC* strain, the R4*Tma* mutant cell population contained more four-
272 *oriC* cells and fewer eight-*oriC* cells, and showed severe asynchronous initiation. Notably, these
273 negative effects of the R4*Tma* mutation were amplified by deletion of *priC*, i.e., the number of one to
274 three-*oriC* cells increased and the ori/mass ratio was further reduced.

275 We next analyzed the role of PriC in cells lacking the AT-L region of *oriC* (subATL *oriC*)
276 (Figure 6A). L-DUE and the flanking AT region assist in DnaB helicase loading by stimulating *oriC*
277 unwinding, which is essential in a strain defective in Right-DnaA subcomplex formation (Sakiyama et
278 al., 2022). SubATL *oriC* cells and WT *oriC* cells formed colonies with similar efficiency on LB agar
279 plates between 25°C and 37°C, regardless of the presence of Δ*priC* (Figure 6B). However, flow
280 cytometry analysis revealed that deletion of *priC* specifically inhibited initiation in subATL *oriC* cells
281 (Figure 6C); the number of eight-*oriC* cells was lower while the number of four-to-seven *oriC* cells was
282 higher in subATL *oriC* Δ*priC* cells than in subATL *oriC* cells with WT *priC.* Taken together, these
283 results are consistent with the idea that PriC restores initiation and DnaB loading at such truncated *oriC*
284 sequences.
285
286 **PriC loads DnaB at *oriC* unwound by the DnaA complex in an *in vitro* reconstituted system.**
287 To analyze the mechanism of PriC rescue of blocked initiation at *oriC*, we assessed PriC activity
288 in an *in vitro* reconstituted system for DnaB loading and DnaB-promoted DNA unwinding using the
289 supercoiled circular form (form I) of the *oriC* plasmid pBS*oriC* and purified proteins, namely DnaA, N-
290 terminally histidine-tagged DnaB (His-DnaB), DnaC, IHF, SSB, and gyrase. In this system, DnaA and
291 IHF unwind the DUE and stimulate His-DnaB loading to the ssDUE region with the aid of DnaC. The
292 loaded His-DnaB expands the ssDNA regions in concert with the ssDNA-binding activities of SSB.
293 Concomitantly, the positive supercoiling generated through DNA unwinding by His-DnaB is resolved by
294 DNA gyrase, resulting in the formation of plasmid DNA topoisomers (form I*). Form I* can be separated
295 from form I by agarose gel electrophoresis (Sakiyama et al., 2018, 2022).
296 First, we assessed the effect of PriC on WT DnaA. WT DnaA stimulated form I* formation in
297 the absence of PriC (Figure 7A, lanes 1 and 5) and increasing concentrations of PriC moderately
298 inhibited WT DnaA-mediated form I* formation (Figure 7A, lanes 5 to 8), probably because of
299 competition between DnaA and PriC for binding to DnaB. Next, we focused on the DnaA F46A H136A
300 double mutant. The DnaA F46A and DnaA H136A mutant proteins alone are reported not to support
301 form I* formation (Keyamura et al., 2009; Sakiyama et al., 2018). Consistently, the DnaA F46A H136A
302 double mutant protein was inactive in form I* formation (Figure 7A, lane 9). However, when PriC was
303 added to the assay, DnaA F46A H136A promoted form I* formation to a level comparable to that of WT
304 DnaA in the presence of PriC (Figure 7A, lanes 5-12 and 7B), indicating that PriC rescues defective
305 DnaB loading by DnaA F46A H136A-*oriC* complexes. These findings are consistent with the idea that
306 PriC can bypass the strict reliance on DnaA-DnaB interactions for DnaB loading at *oriC*.
307 To corroborate this idea, we also determined whether PriC rescues blocked initiation resulting
308 from unstable DUE unwinding. *oriC* complexes containing DnaA V211A cannot bind to the ssDUE and

309 consequently fails in stable DUE unwinding (Ozaki et al., 2008). The DnaA V211A mutant was
310 virtually inactive for form I * formation irrespective of the presence or absence of PriC (Figure 7A,
311 lanes 13-16, and 7B), indicating that PriC cannot efficiently rescue a defect of DUE unwinding.
312 We further evaluated the DnaB loading activity of PriC in the presence of DiaA using a similar
313 *in vitro* reconstituted system. Previously, DiaA was shown to stimulate *oriC* DUE unwinding, but to
314 inhibit form I* formation, because DiaA-DnaA binding competitively inhibits DnaB-DnaA binding; DiaA
315 and DnaB share the same binding site in DnaA domain I (Figures 7C lanes 1, 3, 5, and 7 and 7D)
316 (Keyamura et al., 2009). PriC moderately stimulated form I* formation specifically in the presence of
317 both DnaA and DiaA (Figures 7C lanes 7 and 8, and 7D). These results further support the idea that PriC
318 can bypass the specific requirement for the DnaA-DnaB interaction in DnaB loading at *oriC*. DiaA bound
319 to *oriC*-DnaA complexes might be a physical obstacle reducing efficiency of DnaB loading by PriC.
320 In addition, we analyzed the DUE unwinding activities of DnaA mutants using the *in vitro*
321 reconstituted system. As previously reported, DnaA V211A is largely inactive in DUE unwinding, but
322 DnaA F46A H136A unwinds the DUE at a level comparable to that of WT DnaA (Figure 7-figure
323 supplement 2A and 2B). PriC did not stimulate DUE unwinding irrespective of the presence of WT
324 DnaA (Figure 7-figure supplement 2C and 2D). These results demonstrate the functional specificity of
325 PriC in rescuing failed DnaB loading at *oriC* ssDNA and are consistent with the PriC mechanism
326 mentioned above.
327
328 **Role for PriC in cSDR**
329 Finally, to analyze the role of PriC in other types of replication initiation, we examine whether
330 PriC contributes to the initiation of cSDR, which does not require *dnaA* or *oriC* and is activated in cells
331 lacking *rnhA* or *recG*. Although the PriA-PriB-DnaT primosome complex has previously been reported
332 to be involved in the initiation of cSDR (Heller & Marians, 2006), it is unclear whether PriC has any
333 role in this type of initiation.
334 Unlike *dnaA46* cells, *dnaA46 rnhA*::*cat* double mutant cells formed colonies even at 40°C
335 (Figure 8A), indicating that these cells were engaged in cSDR, as previously reported (Hinds & Sandler,
336 2004). The formation of colonies by Δ*priC dnaA46 rnhA*::*cat* triple mutant cells was severely inhibited
337 at 40°C (Figure 8A), suggesting that PriC contributes to the growth of *dnaA46 rnhA*::*cat* mutant cells.
338 To determine whether PriC contributes to the initiation of *dnaA46-oriC* replication or cSDR,
339 we calculated the relative ratios of *oriC* (84.6 min) and *ter* (32.4 min) copy numbers to the refence
340 locus *yapB* (50.5 min) copy number using real-time quantitative PCR (qPCR). To calculate the copy
341 number of the chromosomal *ter* region, the preferential initiation site of cSDR (Maduike et al., 2014),
342 *dnaA46 rnhA*::*cat* cells growing exponentially at 30°C were shifted to 40°C for 90 min and the copy

343 number before and after incubation at 40°C was calculated. Consistent with the colony formation data
344 (Figure 8A), the *ter* copy number ratio of the *dnaA46 rnhA*::*cat* double mutant increased after 40°C
345 incubation, whereas the copy number ratio of the *dnaA46* mutant expressing WT *rnhA* remained the
346 same. The *ter* copy number ratio of the *dnaA46 rnhA*::*cat* Δ*priC* triple mutant strain was also increased,
347 indicating that cSDR could occur even in the absence of PriC.
348 To monitor initiation of DnaA-*oriC* replication, we determined the *oriC* copy number ratio
349 (Figure 8B). At the permissive temperature, the *oriC* copy number ratio of the *dnaA46* Δ*priC* double
350 mutant strain was lower than that of the *dnaA46* single mutant, confirming the importance of PriC for
351 replication initiation in *dnaA46* cells, as shown in Figure 2. In the *dnaA46 rnhA*::*cat* double mutant
352 expressing WT *priC*, the *oriC* copy number ratio was reduced, which is explained by activation of
353 cSDR and increase of the relative copy number of the reference *yapB* locus (50.5 min chromosomal
354 map position). Together, these results suggest the idea that PriC stimulates replication fork progression
355 during cSDR.
356
357 **Discussion**
358 In growing cells, replication initiation can be blocked under challenging conditions. However,
359 the mechanisms that rescue blocked initiations are largely unknown. To elucidate such mechanisms, we
360 investigated PriC-promoted replication initiation under various challenging conditions. We showed that
361 PriC was necessary for the optimal growth of *dnaC2* cells at the semi-restrictive temperature and for
362 replication initiation even at the permissive temperature (Figure 2), suggesting that PriC contributes to
363 replication initiation rescue in *dnaC2* cells by facilitating DnaB helicase loading at *oriC*. Furthermore,
364 we observed that PriC was necessary for the optimal growth of cells in which the DnaA-DnaB
365 interaction was inhibited by DiaA overexpression or DnaA F46A H136A double mutations (Figures 3
366 and 4). In addition, PriC was stimulatory for the colony formation and replication initiation bearing
367 *oriC* mutations that impair efficient DnaB loading (Figures 5 and 6). These results, together with results
368 of form I* formation assays (Figures 7), suggest that PriC bypasses the need for the DnaA-DnaB
369 interaction by binding to unwound *oriC* DNA and recruiting DnaB to facilitate its loading onto ssDNA
370 (Figure 9). This mechanism is similar to that proposed for the rescue of abandoned replication forks by
371 PriC (Figure 1E).
372 The finding that PriC failed to stimulate form I* formation in the presence of DnaA V211A,
373 which lacks DUE unwinding activity (Figures 7), provides mechanistic insight into PriC-dependent
374 replication initiation at *oriC*. We propose that PriC-dependent replication initiation possibly begins with
375 the recognition of a stably unwound ssDNA region by PriC (Figure 9). Consistent with this perspective,
376 PriC ssDNA-binding activity and ssDNA regions have been reported to be important for PriC-promoted

377 replication fork rescue (Heller & Marians, 2006; McMillan & Keck, 2024). The failure of PriC to
378 stimulate replication initiation in Δ*diaA* cells (Figure 4C) is also potentially explained by the reduced
379 DUE unwinding caused by destabilization of the DnaA-*oriC* complex in Δ*diaA* cells. Based on this, we
380 suggest that the stably unwound ssDNA region in *oriC* serves as a distinctive feature for PriC-
381 promoting DnaB loading at *oriC* for replication initiation rescue, and distinguishes it from PriA-
382 dependent replication restart, which requires the structure of the replication fork DNA consisting of
383 sister dsDNA strands (Heller & Marians, 2005a; Windgassen et al., 2018).
384 In this study, we found that cells with DnaA F46A H136A double mutations grew well, but
385 only when the cells expressed WT PriC, whereas the growth of cells expressing the DnaA H136A single
386 mutant was severely inhibited even when the cells expressed WT PriC (Sakiyama et al., 2018). The
387 His136 residue is located within the weak, secondary DnaB interaction region in DnaA, and is crucial
388 for DnaB loading onto *oriC* ssDNA. Although domain I in DnaA H136A can stably tether DnaB-DnaC
389 complexes to DnaA complexes on *oriC* (Sakiyama et al., 2018), the complexes fail to load DnaB onto
390 *oriC* ssDNA even in the presence of PriC. It is possible that the interaction between PriC and DnaB is
391 inhibited by DnaB binding to DnaA domain I. Conversely, the PriC-DnaB interaction may inhibit the
392 interaction between DnaA domain I and DnaB, as suggested by the inhibitory effect of PriC on DnaB
393 loading *in vitro* in the presence of WT DnaA (Figure 7). However, this inhibitory effect of PriC was not
394 observed *in vivo*, suggesting that PriC-DnaB binding could involve still unknown factors and regulatory
395 mechanisms.
396 PriC supported cSDR-dependent growth in *dnaA46 rnhA*::*cat* double mutant cells without
397 stimulating the initiation of cSDR (Figure 8). In this mutant, cSDR predominantly initiates from the *ter*
398 region, resulting in head-on collisions between the replisome and transcription complexes in *rrn*
399 operons (Maduike et al., 2014). This suggests that in cSDR cells PriC specifically rescues abandoned
400 forks including those generated during head-on conflicts between the replisome and transcription
401 complexes.
402 *Bacillus subtilis* (*B. subtilis*), which expresses a PriA homolog but not a PriC homolog,
403 employs a PriA-independent fork rescue pathway (Bruand et al., 2001). In this pathway, *B. subtilis*
404 DnaC (*Bsu*DnaC) helicase is reloaded using the helicase loader DnaI together with *B. subtilis* DnaB
405 (*Bsu*DnaB) and DnaD coloaders. The ssDNA-binding activity of *Bsu*DnaB has a crucial role in this
406 PriA-independent pathway (Bruand et al., 2005). SsDNA-bound *Bsu*DnaB remodels the SSB-ssDNA
407 complex with DnaD and recruits *Bsu*DnaC. These functions of *Bsu*DnaB are similar to the proposed
408 functions of PriC in replication fork rescue in *E. coli*. In addition, *Bsu*DnaC helicase is recruited to *oriC*
409 by concerted actions of *B. subtilis* DnaA and the DnaD-*Bsu*DnaB complex, which has an essential role
410 in chromosome replication initiation (Jameson & Wilkinson, 2017), suggesting a similar role of

411 *Bsu*DnaB to PriC in *E. coli* cells expressing DnaA F46A H136A. These similarities between PriC and
412 *Bsu*DnaB in these two evolutionarily distant bacterial species suggest that the mechanism of PriC-
413 promoted helicase loading is conserved among bacterial species despite the absence of sequence
414 conservation of PriC and *Bsu*DnaB homologs.

415 Based on our results, we propose the abnormal competition between DnaB and DiaA for
416 DnaA domain I could represent a form of intrinsic replication initiation stress in bacteria with conserved
417 DiaA homologs. This type of stress could also occur in ε-proteobacterial species, such as *Helicobacter*
418 *pylori*, because they express HobA, a DiaA-functional homolog (Natrajan et al., 2007; Zawilak-Pawlik
419 et al., 2011). Similarly, YfdR, encoded by *E. coli* prophages, inhibits replication initiation by competing
420 with DnaB for binding to DnaA domain I (Noguchi & Katayama, 2016), suggesting that such
421 extraneously introduced inhibitors could trigger replication initiation stress.

422 Even in human, ORC1, ORC2, and ORC5, the essential components of the eukaryotic
423 replication initiation complex, are not essential in some cancer cell-lines (Shibata & Dutta, 2020; Struhl
424 et al., 2016), suggesting that mechanisms of replication initiation rescue may also operate beyond the
425 bacterial kingdom. Therefore, further investigation of the initiation rescue processes and the factors
426 involved in diverse organisms from bacteria to human will be important for a full understanding of the
427 common principles and diverse mechanisms that ensure robust initiation of chromosomal DNA
428 replication.

429

430 **Materials and Methods**

431 **Plasmids, proteins, and strains**

432 The plasmids used in this study are listed in Key Resource Table. pKA234, pKW44-1, pNA135,
433 pBS*oriC*, pET22b(+)-priC, and pTKM601 were described previously (Aramaki et al., 2015; Ishida et
434 al., 2004; Kawakami et al., 2005; Keyamura et al., 2009; Kubota et al., 1997; Ozaki et al., 2008). For
435 the construction of pFH, an alanine substitution was introduced into pH136A with specific mutagenic
436 primer sets using the QuikChange site-directed mutagenesis protocol (Stratagene [Agilent], Agilent, La
437 Jolla, CA, United States) as described previously (Keyamura et al., 2007; Sakiyama et al., 2018).

438 WT DnaA and its derivative proteins were overproduced in *E. coli* strain KA450 from pKA234,
439 pKW44-1, or pFH and purified as described previously (Noguchi et al., 2015; Ozaki et al., 2008;
440 Sakiyama et al., 2017).

441 PriC protein was prepared as previously reported with minor modifications (Aramaki et al., 2013).
442 Briefly, PriC protein was overproduced in *E. coli* strain BL21-codonPlus-RIL by inducing its
443 expression from pET22b(+)-priC using 0.2 mM isopropyl-β-D-1-thiogalactopyranoside (IPTG). The
444 resulting cells were suspended in chilled buffer A (50 mM HEPES-NaOH [pH7.0], 10% sucrose, 1 mM

445 EDTA, 2 mM dithiothreitol (DTT), and 1 mM PMSF) and disrupted by sonication. Proteins in the
446 soluble fraction were precipitated with 0.24 g/mL ammonium sulfate, resuspended in a separation buffer
447 (50 mM imidazole [pH 7.0], 20% glycerol, 2 mM DTT, 1 mM EDTA, and 40 mM ammonium sulfate)
448 and loaded onto a 1 mL HiTrap® SP HP column (Cytiva, Uppsala, Sweden). Bound proteins were
449 eluted with a linear gradient from 0 to 1 M sodium chloride.
450 All *E. coli* strains used in this study are listed in Key Resource Table. KYA018, MIT125,
451 MIT162, SA103, NY20 and NY21 were described previously (Kasho & Katayama, 2013; Noguchi et
452 al., 2015; Noguchi & Katayama, 2016). Strains bearing mutant *oriC* (NY20L and NY20ATL) were
453 constructed using the λRed site-directed recombination system as previously described (Noguchi et al.,
454 2015; Sakiyama et al., 2017, 2022). NY20-frt strain and *oriC* mutant strains (NY21-frt, NY20L-frt, and
455 NY20ATL-frt) were constructed by eliminating *kan* from the NY20 strain and strains NY21, NY20L,
456 and NY20ATL. To remove the kanamycin-resistant cassette (*kan*) from *oriC*, FLP recombinase encoded
457 on pCP20 was used. Elimination of *kan* was verified by checking sensitivity to 50 μg/ml kanamycin in
458 LB agar plates.
459 Δ*priC*::*frt-kan* from JW0456-KC and Δ*rep*::*frt-kan* from JW5604-KC were introduced into
460 MG1655 by P1 transduction, resulting in the construction of KRC002 and FF001, respectively. For
461 construction of other Δ*priC*::*frt-kan* strains (KRC004, KRC005, NY20-*priC*, NY21-*priC*, NY20L-*priC*,
462 NY20ATL-*priC*), P1 phage lysates prepared from KRC002 were used for transduction of strains
463 MIT125, KYA018, NY20-frt, SYM21-frt, NY20L-frt, and NY20ATL-frt. Transductants were screened
464 on LB agar plates containing 50 μg/mL kanamycin. Δ*diaA*::*frt-kan* or *rnhA*::*cat* derivatives (KRC006,
465 MIT125c, and KRC004c) were constructed using a similar protocol except that P1 phage lysates from
466 SA103 (Δ*diaA*::*frt-kan*) or MIT162 (*rnhA*::*cat*) were used. KRC003 was generated by removal of *kan*
467 from KRC002.
468
469 **Buffers**
470 Buffer P contained 60 mM HEPES–KOH (pH 7.6), 0.1 mM zinc acetate, 8 mM magnesium
471 acetate, 30% [v/v] glycerol, and 0.32 mg/mL bovine serum albumin (BSA). Buffer N contained 50 mM
472 HEPES–KOH (pH 7.6), 2.5 mM magnesium acetate, 0.3 mM EDTA, 7 mM DTT, 0.007% [v/v] Triton
473 X-100, and 20% [v/v] glycerol. Form I* buffer contained 20 mM Tris-HCl (pH 7.5), 125 mM potassium
474 glutamate, 10 mM magnesium acetate, 8 mM DTT, and 0.5 mg/mL BSA.
475
476 **DUE unwinding assay**
477 DUE unwinding assays were performed essentially as described with minor modifications
478 (Sakiyama et al., 2022; Yoshida et al., 2023). Briefly, DnaA was incubated with ATP in buffer N on ice

479 for 3 min to generate ATP-DnaA. The indicated amount of PriC and ATP-DnaA or its mutant derivatives
480 was incubated for 9 min at 30°C in 10 μL buffer P containing 5 mM ATP, 125 mM potassium glutamate,
481 1.6 nM pBS*oriC*, and 42 nM IHF, followed by further incubation with 1.5 units of P1 nuclease (Wako)
482 for 5 min. The reaction was stopped by the addition of 1% SDS and 25 mM EDTA, and DNA was
483 purified by phenol-chloroform extraction and ethanol precipitation. One-third of each purified DNA
484 was digested with AlwNI (NEB), which yielded 2.6 kb and 1.0 kb fragments after DUE unwinding of
485 pBS*oriC*. The resultant DNA fragments were analyzed by 1% agarose gel electrophoresis with 1xTris-
486 acetate-EDTA buffer for 30 min at 100 V, followed by ethidium bromide staining. Gel images were
487 taken using the GelDoc GO imaging system (Bio-Rad Laboratories, Hercules, CA), and products
488 derived from unwound plasmids were quantified using ImageJ software.
489
490 **Form I* assay**
491 This assay was performed as previously described with minor modifications (Noguchi et al.,
492 2015; Sakiyama et al., 2022). The indicated amount of ATP-DnaA was incubated for 15 min at 30°C in
493 12.5 μL of Form I* buffer containing 3 mM ATP, 1.6 nM pBS*oriC*, 42 nM IHF, 400 nM His-DnaB, 400
494 nM DnaC, 76 nM GyrA, 100 nM His-GyrB, and 760 nM SSB. The reaction was stopped by the
495 addition of 0.5% SDS, and DNA was purified by phenol-chloroform extraction. Samples were analyzed
496 by 0.65% agarose gel electrophoresis with 0.5xTris-borate-EDTA buffer for 15 h at 23 V, followed by
497 ethidium bromide staining.
498
499 **Flow cytometry analysis**
500 Flow cytometry analysis was performed essentially as described (Kasho et al., 2014). Briefly,
501 cells were grown at 30°C in LB medium until the absorbance of the culture (A_{600}) reached 0.1. Portions
502 of the cultures were diluted a thousand-fold into 5 ml LB medium and incubated at 30°C until the
503 absorbance of the culture (A600) reached 0.1. The remaining portions were further incubated to
504 determine the doubling time (Td) by measuring A_{600} every 20 min. At A_{600} 0.1, aliquots of the cultures
505 were fixed in 70% ethanol to analyze cell mass using the Multisizer 3 Coulter counter (Beckman
506 Coulter, Brea, CA). The remaining cultures were further incubated for 4 h with 0.3 mg/mL rifampicin
507 and 0.01 mg/mL cephalexin to allow run-out replication of chromosomal DNA. The resultant cells were
508 fixed in 70% ethanol. After DNA staining with SYTOX Green (Thermo Fisher Scientific, Waltham,
509 MA), cellular DNA contents were analyzed on a FACS Calibur flow cytometer (BD Bioscience,
510 Franklin Lakes, NJ). The number of the origins/cell (ori/cell) was determined from the histograms of
511 flow cytometry analysis. The number of ori/cell was divided by the mean cell mass determined by cell
512 mass analysis, resulting in ori/mass ratios. The numbers of cells containing non-2^n copy number of *oriC*

513 were divided by the number of cells containing 2^n copy number of *oriC* to calculate the asynchrony
514 index (A.I.). For the analysis of cells bearing plasmids, LB medium was supplemented with 100 μg/mL
515 ampicillin.
516
517 **Replication initiation frequency test using synchronized cultures**
518 MIT125 (*dnaA46, tnaA*::Tn10) cells or its Δ*priC* derivative KRC004 were grown at 30°C, a
519 permissive temperature, in LB medium until the absorbance of the culture (A_{600}) reached 0.04, followed
520 by further incubation for 90 min at 42°C, a restrictive temperature. Aliquots of the cultures were fixed
521 in 70% ethanol as "Synchronization" samples. The remaining cultures were further incubated for 5 min
522 to initiate DNA replication, followed by further incubation for 4 h at 42°C with 0.3 mg/mL rifampicin
523 and 0.01 mg/mL cephalexin to allow run-out replication of chromosomal DNA. The resultant cells were
524 fixed in 70% ethanol as "5 min release" samples. After DNA staining with SYTOX Green (Life
525 Technologies), cellular DNA contents were analyzed on a FACS Calibur flow cytometer (BD
526 Bioscience). Ratios of the origins/cell (ori/cell) were determined from the histograms of flow cytometry
527 analysis.
528 For synchronization of *dnaC2* mutant cells (KYA018 and KRC005), cells were grown in LB
529 medium at 30°C until the A_{600} reached 0.04, followed by further incubation for 80 min at 37°C, at the
530 restrictive temperature. The resulting synchronized cultures were released for 5 min at 30°C and
531 incubated in the presence of 0.3 mg/mL rifampicin and 0.01 mg/mL cephalexin at 30°C to allow run-out
532 of chromosomal DNA replication.
533
534 **qPCR for analysis of cSDR**
535 Cells of MIT125 (*dnaA46, tnaA*::Tn10), MIT125c (*dnaA46, tnaA*::Tn10, *rnhA*::*cat*) and its
536 Δ*priC* derivatives KRC004 (*dnaA46, tnaA*::Tn10, Δ*priC*::*frt-kan*) and KRC004c (*dnaA46, tnaA*::Tn10,
537 *rnhA*::*cat*, Δ*priC*::*frt-kan*) were grown at 30°C in LB medium until the absorbance of the culture (A_{600})
538 reached 0.04 and aliquots of the cultures were withdrawn. The remaining samples were further
539 incubated for 90 min at 40°C and aliquots of the cultures were withdrawn. These samples were boiled
540 for 5 min at 95°C and the genome DNA was extracted. The levels of *oriC* (84.6 min), *ter* (32.4 min),
541 and *yapB* (50.5 min) were quantified by real-time qPCR using TB Green Premix Ex TaqII (Tli RNaseH
542 Plus) (TaKaRa, Shiga, Japan) and the following primers: ORI_1 and KWoriCRev for *oriC*, qoriK fw and
543 qoriK rev for *ter*, STM419 and STM420 for *yapB*.
544
545
546 **Acknowledgments**

We are grateful to Dr. Yoshio Abe for discussion and *priC*-overproducing plasmid, to Drs. Yusuke Akama and Yukari Sakiyama for initial exploratory study related to this work, and to NRBP-E. coli at NIG for bacterial strains.

Fundings

Japan Society for the Promotion of Science (JSPS KAKENHI) [JP17H03656, JP20H03212 and JP23K27131].

References

Abe, Y., Jo, T., Matsuda, Y., Matsunaga, C., Katayama, T., & Ueda, T. (2007). Structure and function of DnaA N-terminal domains: Specific sites and mechanisms in inter-DnaA interaction and in DnaB helicase loading on *oriC*. *Journal of Biological Chemistry*, *282*(24), 17816–17827. https://doi.org/10.1074/jbc.M701841200

Aramaki, T., Abe, Y., Furutani, K., Katayama, T., & Ueda, T. (2015). Basic and aromatic residues in the C-terminal domain of PriC are involved in ssDNA and SSB binding. *Journal of Biochemistry*, *157*(6), 529–537. https://doi.org/10.1093/jb/mvv014

Aramaki, T., Abe, Y., Ohkuri, T., Mishima, T., Yamashita, S., Katayama, T., & Ueda, T. (2013). Domain separation and characterization of PriC, a replication restart primosome factor in *Escherichia coli*. *Genes to Cells*, *18*(9), 723–732. https://doi.org/10.1111/gtc.12069

Arias-Palomo, E., Puri, N., O'Shea Murray, V. L., Yan, Q., & Berger, J. M. (2019). Physical Basis for the Loading of a Bacterial Replicative Helicase onto DNA. *Molecular Cell*, *74*(1), 173-184.e4. https://doi.org/10.1016/j.molcel.2019.01.023

Asai, T., & Kogomal, T. (1994). MINIREVIEW D-Loops and R-Loops: Alternative Mechanisms for the Initiation of Chromosome Replication in *Escherichia coli*. *JOURNAL OF BACTERIOLOGY*, *176*(7), 1807–1812. https://journals.asm.org/journal/jb

Bruand, C., Farache, M., McGovern, S., Ehrlich, S. D., & Polard, P. (2001). DnaB, DnaD and DnaI proteins are components of the *Bacillus subtilis* replication restart primosome. *Molecular Microbiology*, *42*(1), 245–256. https://doi.org/10.1046/j.1365-2958.2001.02631.x

Bruand, C., Velten, M., McGovern, S., Marsin, S., Sérèna, C., Dusko Ehrlich, S., & Polard, P. (2005). Functional interplay between the *Bacillus subtilis* DnaD and DnaB proteins essential for initiation and re-initiation of DNA replication. *Molecular Microbiology*, *55*(4), 1138–1150. https://doi.org/10.1111/j.1365-2958.2004.04451.x

Chodavarapu, S., & Kaguni, J. M. (2016). Replication Initiation in Bacteria. *Enzymes*, *39*, 1–30. https://doi.org/10.1016/bs.enz.2016.03.001

Costa, A., & Diffley, J. F. X. (2022). The Initiation of Eukaryotic DNA Replication. *Annu. Rev. Biochem*, *91*,

107–131. https://doi.org/10.1146/annurev-biochem-072321

Duckworth, A. T., Ducos, P. L., McMillan, S. D., Satyshur, K. A., Blumenthal, K. H., Deorio, H. R., Larson, J. A., Sandler, S. J., Grant, T., & Keck, J. L. (2023). Replication fork binding triggers structural changes in the PriA helicase that govern DNA replication restart in *E. coli*. *Nature Communications*, *14*(1), 1–13. https://doi.org/10.1038/s41467-023-38144-x

Duderstadt, K. E., Chuang, K., & Berger, J. M. (2011). DNA stretching by bacterial initiators promotes replication origin opening. *Nature*, *478*(7368), 209–213. https://doi.org/10.1038/nature10455

Erzberger, J. P., Mott, M. L., & Berger, J. M. (2006). Structural basis for ATP-dependent DnaA assembly and replication-origin remodeling. *Nature Structural and Molecular Biology*, *13*(8), 676–683. https://doi.org/10.1038/nsmb1115

Fang, L., Davey, M. J., & O'donnell, M. (1999). Replisome Assembly at *oriC*, the Replication Origin of *E. coli*, Reveals an Explanation for Initiation Sites outside an Origin. *Molecular Cell*, *4*, 541–553.

Felczak, M. M., & Kaguni, J. M. (2004). The box VII motif of *Escherichia coli* DnaA protein is required for DnaA oligomerization at the *E. coli* replication origin. *Journal of Biological Chemistry*, *279*(49), 51156–51162. https://doi.org/10.1074/jbc.M409695200

Flores, M. J., Ehrlich, S. D., & Michel, B. (2002). Primosome assembly requirement for replication restart in the *Escherichia coli holDG10* replication mutant. *Molecular Microbiology*, *44*(3), 783–792. https://doi.org/10.1046/j.1365-2958.2002.02913.x

Fujikawa, N., Kurumizaka, H., Nureki, O., Terada, T., Shirouzu, M., Katayama, T., & Yokoyama, S. (2003). Structural basis of replication origin recognition by the DnaA protein. *Nucleic Acids Research*, *31*(8), 2077–2086. https://doi.org/10.1093/nar/gkg309

Grimwade, J. E., & Leonard, A. C. (2021). Blocking, Bending, and Binding: Regulation of Initiation of Chromosome Replication During the *Escherichia coli* Cell Cycle by Transcriptional Modulators That Interact With Origin DNA. In *Frontiers in Microbiology* (Vol. 12, p. 732270). Frontiers Media S.A. https://doi.org/10.3389/fmicb.2021.732270

Hayashi, C., Miyazaki, E., Ozaki, S., Abe, Y., & Katayama, T. (2020). DnaB helicase is recruited to the replication initiation complex via binding of DnaA domain I to the lateral surface of the DnaB N-terminal domain. *Journal of Biological Chemistry*, *295*(32), 1131–1143. https://doi.org/10.1074/jbc.ra120.014235

Heller, R. C., & Marians, K. J. (2005a). The disposition of nascent strands at stalled replication forks dictates the pathway of replisome loading during restart. *Molecular Cell*, *17*(5), 733–743. https://doi.org/10.1016/j.molcel.2005.01.019

Heller, R. C., & Marians, K. J. (2005b). Unwinding of the nascent lagging strand by Rep and PriA enables the direct restart of stalled replication forks. *Journal of Biological Chemistry*, *280*(40), 34143–34151. https://doi.org/10.1074/jbc.M507224200

Heller, R. C., & Marians, K. J. (2006). Replication fork reactivation downstream of a blocked nascent leading strand. *Nature*, *439*(7076), 557–562. https://doi.org/10.1038/nature04329

Hinds, T., & Sandler, S. J. (2004). Allele specific synthetic lethality between *priC* and *dnaAts* alleles at the permissive temperature of 30°C in *E. coli* K-12. *BMC Microbiology*, *4*, 1–9.

https://doi.org/10.1186/1471-2180-4-47

Ishida, T., Akimitsu, N., Kashioka, T., Hatano, M., Kubota, T., Ogata, Y., Sekimizu, K., & Katayama, T. (2004). DiaA, a novel DnaA-binding protein, ensures the timely initiation of *Escherichia coli* chromosome replication. *Journal of Biological Chemistry*, *279*(44), 45546–45555. https://doi.org/10.1074/jbc.M402762200

Jameson, K. H., & Wilkinson, A. J. (2017). Control of initiation of DNA replication in *Bacillus subtilis* and *Escherichia coli*. In *Genes* (Vol. 8, Issue 1, p. 22). MDPI AG. https://doi.org/10.3390/genes8010022

Kasho, K., Fujimitsu, K., Matoba, T., Oshima, T., & Katayama, T. (2014). Timely binding of IHF and Fis to *DARS2* regulates ATP-DnaA production and replication initiation. *Nucleic Acids Research*, *42*(21), 13134–13149. https://doi.org/10.1093/nar/gku1051

Kasho, K., & Katayama, T. (2013). DnaA binding locus *datA* promotes DnaA-ATP hydrolysis to enable cell cycle-coordinated replication initiation. *Proceedings of the National Academy of Sciences of the United States of America*, *110*(3), 936–941. https://doi.org/10.1073/pnas.1212070110

Kasho, K., Ozaki, S., & Katayama, T. (2023). IHF and Fis as *Escherichia coli* Cell Cycle Regulators: Activation of the Replication Origin *oriC* and the Regulatory Cycle of the DnaA Initiator. In *International Journal of Molecular Sciences* (Vol. 24, Issue 14, p. 11572). Multidisciplinary Digital Publishing Institute (MDPI). https://doi.org/10.3390/ijms241411572

Kawakami, H., Keyamura, K., & Katayama, T. (2005). Formation of an ATP-DnaA-specific initiation complex requires DnaA arginine 285, a conserved motif in the AAA+ protein family. *Journal of Biological Chemistry*, *280*(29), 27420–27430. https://doi.org/10.1074/jbc.M502764200

Keyamura, K., Abe, Y., Higashi, M., Ueda, T., & Katayama, T. (2009). DiaA dynamics are coupled with changes in initial origin complexes leading to helicase loading. *Journal of Biological Chemistry*, *284*(37), 25038–25050. https://doi.org/10.1074/jbc.M109.002717

Keyamura, K., Fujikawa, N., Ishida, T., Ozaki, S., Su'etsugu, M., Fujimitsu, K., Kagawa, W., Yokoyama, S., Kurumizaka, H., & Katayama, T. (2007). The interaction of DiaA and DnaA regulates the replication cycle in *E. coli* by directly promoting ATP-DnaA-specific initiation complexes. *Genes and Development*, *21*(16), 2083–2099. https://doi.org/10.1101/gad.1561207

Kogoma, T. (1997). Stable DNA Replication: Interplay between DNA Replication, Homologous Recombination, and Transcription. *MICROBIOLOGY AND MOLECULAR BIOLOGY REVIEWS*, *61*(2), 212–238. https://journals.asm.org/journal/mmbr

Kubota, T., Katayama, T., Ito, Y., Mizushima, T., & Sekimizu, K. (1997). Conformational Transition of DnaA Protein by ATP: Structural Analysis of DnaA Protein, the Initiator of *Escherichia coli* Chromosome Replication. *BIOCHEMICAL AND BIOPHYSICAL RESEARCH COMMUNICATIONS*, *232*, 130–135.

Lopper, M., Boonsombat, R., Sandler, S. J., & Keck, J. L. (2007). A Hand-Off Mechanism for Primosome Assembly in Replication Restart. *Molecular Cell*, *26*(6), 781–793. https://doi.org/10.1016/j.molcel.2007.05.012

Maduike, N. Z., Tehranchi, A. K., Wang, J. D., & Kreuzer, K. N. (2014). Replication of the *Escherichia coli* chromosome in RNase HI-deficient cells: Multiple initiation regions and fork dynamics. *Molecular Microbiology*, *91*(1), 39–56. https://doi.org/10.1111/mmi.12440

Masai, H., Asai, T., Kubota, Y., Arai, K. I., & Kogoma, T. (1994). *Escherichia coli* PriA protein is essential for inducible and constitutive stable DNA replication. *EMBO Journal*, *13*(22), 5338–5345. https://doi.org/10.1002/j.1460-2075.1994.tb06868.x

McMillan, S. D., & Keck, J. L. (2024). Biochemical characterization of *Escherichia coli* DnaC variants that alter DnaB helicase loading onto DNA. *Journal of Biological Chemistry*, *300*(5), 107275. https://doi.org/10.1016/j.jbc.2024.107275

Michel, B., & Sandler, S. J. (2017). Replication restart in bacteria. In *Journal of Bacteriology* (Vol. 199, Issue 13, pp. e00102-17). American Society for Microbiology. https://doi.org/10.1128/JB.00102-17

Miller, D. T., Grimwade, J. E., Betteridge, T., Rozgaja, T., Torgue, J.-C., Leonard, A. C., & Helinski, D. R. (2009). Bacterial origin recognition complexes direct assembly of higher-order DnaA oligomeric structures. *Proceedings of the National Academy of Sciences of the United States of America*, *106*(44), 18479–18484. www.pnas.orgcgidoi10.1073pnas.0909472106

Nagata, K., Okada, A., Ohtsuka, J., Ohkuri, T., Akama, Y., Sakiyama, Y., Miyazaki, E., Horita, S., Katayama, T., Ueda, T., & Tanokura, M. (2020). Crystal structure of the complex of the interaction domains of *Escherichia coli* DnaB helicase and DnaC helicase loader: Structural basis implying a distortion-accumulation mechanism for the DnaB ring opening caused by DnaC binding. *Journal of Biochemistry*, *167*(1), 1–14. https://doi.org/10.1093/jb/mvz087

Natrajan, G., Hall, D. R., Thompson, A. C., Gutsche, I., & Terradot, L. (2007). Structural similarity between the DnaA-binding proteins HobA (HP1230) from *Helicobacter pylori* and DiaA from *Escherichia coli*. *Molecular Microbiology*, *65*(4), 995–1005. https://doi.org/10.1111/j.1365-2958.2007.05843.x

Né Dicte Michel, B., Flores, M.-J., Viguera, E., Grompone, G., Seigneur, M., & Bidnenko, V. (2001). Rescue of arrested replication forks by homologous recombination. *Proceedings of the National Academy of Sciences of the United States of America*, *17*(15), 8181–8188. www.pnas.orgcgidoi10.1073pnas.111008798

Nguyen, B., Shinn, M. K., Weiland, E., & Lohman, T. M. (2021). Regulation of *E. coli* Rep helicase activity by PriC. *Journal of Molecular Biology*, *433*(15), 167072. https://doi.org/10.1016/j.jmb.2021.167072

Noguchi, Y., & Katayama, T. (2016). The *Escherichia coli* cryptic prophage protein YfdR binds to DnaA and initiation of chromosomal replication is inhibited by overexpression of the gene cluster *yfdQ-yfdR-yfdS-yfdT*. *Frontiers in Microbiology*, *7*(MAR), 1–21. https://doi.org/10.3389/fmicb.2016.00239

Noguchi, Y., Sakiyama, Y., Kawakami, H., & Katayama, T. (2015). The Arg fingers of key DnaA protomers are oriented inward within the replication origin *oriC* and stimulate DnaA subcomplexes in the initiation complex. *Journal of Biological Chemistry*, *290*(33), 20295–20312. https://doi.org/10.1074/jbc.M115.662601

Nozaki, S., & Ogawa, T. (2008). Determination of the minimum domain II size of *Escherichia coli* DnaA protein essential for cell viability. *Microbiology*, *154*(11), 3379–3384. https://doi.org/10.1099/mic.0.2008/019745-0

O'Donnell, M., Langston, L., & Stillman, B. (2013). Principles and concepts of DNA replication in bacteria, archaea, and eukarya. *Cold Spring Harbor Perspectives in Biology*, *5*(7), a010108. https://doi.org/10.1101/cshperspect.a010108

Ozaki, S., & Katayama, T. (2012). Highly organized DnaA-*oriC* complexes recruit the single-stranded DNA for replication initiation. *Nucleic Acids Research*, *40*(4), 1648–1665. https://doi.org/10.1093/nar/gkr832

Ozaki, S., Kawakami, H., Nakamura, K., Fujikawa, N., Kagawa, W., Park, S. Y., Yokoyama, S., Kurumizaka, H., & Katayama, T. (2008). A common mechanism for the ATP-DnaA-dependent formation of open complexes at the replication origin. *Journal of Biological Chemistry*, *283*(13), 8351–8362. https://doi.org/10.1074/jbc.M708684200

Ozaki, S., Noguchi, Y., Hayashi, Y., Miyazaki, E., & Katayama, T. (2012). Differentiation of the DnaA-*oriC* subcomplex for DNA unwinding in a replication initiation complex. *Journal of Biological Chemistry*, *287*(44), 37458–37471. https://doi.org/10.1074/jbc.M112.372052

Rozgaja, T. A., Grimwade, J. E., Iqbal, M., Czerwonka, C., Vora, M., & Leonard, A. C. (2011). Two oppositely oriented arrays of low-affinity recognition sites in *oriC* guide progressive binding of DnaA during *Escherichia coli* pre-RC assembly. *Molecular Microbiology*, *82*(2), 475–488. https://doi.org/10.1111/j.1365-2958.2011.07827.x

Sakiyama, Y., Kasho, K., Noguchi, Y., Kawakami, H., & Katayama, T. (2017). Regulatory dynamics in the ternary DnaA complex for initiation of chromosomal replication in *Escherichia coli*. *Nucleic Acids Research*, *45*(21), 12354–12373. https://doi.org/10.1093/nar/gkx914

Sakiyama, Y., Nagata, M., Yoshida, R., Kasho, K., Ozaki, S., & Katayama, T. (2022). Concerted actions of DnaA complexes with DNA-unwinding sequences within and flanking replication origin *oriC* promote DnaB helicase loading. *Journal of Biological Chemistry*, *298*(6), 102051. https://doi.org/10.1016/j.jbc.2022.102051

Sakiyama, Y., Nishimura, M., Hayashi, C., Akama, Y., Ozaki, S., & Katayama, T. (2018). The DnaA AAA+ Domain His136 residue directs DnaB replicative helicase to the unwound region of the replication origin, *oriC*. *Frontiers in Microbiology*, *9*(AUG), 1–17. https://doi.org/10.3389/fmicb.2018.02017

Sandler, S. J. (2000). Multiple Genetic Pathways for Restarting DNA Replication Forks in *Escherichia coli* K-12. *Genetics*, *155*, 487–497. https://academic.oup.com/genetics/article/155/2/487/6048048

Sandler, S. J., Marians, K. J., Zavitz, K. H., Coutu, J., Parent, M. A., & Clark, A. J. (1999). *dnaC* mutations suppress defects in DNA replication- and recombination-associated functions in *priB* and *priC* double mutants in *Escherichia coli* K-12. *Molecular Microbiology*, *34*(1), 91–101. https://doi.org/10.1046/j.1365-2958.1999.01576.x

Shibata, E., & Dutta, A. (2020). A human cancer cell line initiates DNA replication normally in the absence of ORC5 and ORC2 proteins. *Journal of Biological Chemistry*, *295*(50), 16949–16959. https://doi.org/10.1074/jbc.RA120.015450

Shimizu, M., Noguchi, Y., Sakiyama, Y., Kawakami, H., Katayama, T., & Takada, S. (2016). Near-atomic structural model for bacterial DNA replication initiation complex and its functional insights. *Proceedings of the National Academy of Sciences of the United States of America*, *113*(50), E8021–E8030. https://doi.org/10.1073/pnas.1609649113

Stepankiw, N., Kaidow, A., Boye, E., & Bates, D. (2009). The right half of the *Escherichia coli* replication origin is not essential for viability, but facilitates multi-forked replication. *Molecular Microbiology*,

74(2), 467–479. https://doi.org/10.1111/j.1365-2958.2009.06877.x

Struhl, K., Shibata, E., Kiran, M., Shibata, Y., Singh, S., Kiran, S., & Dutta, A. (2016). Two subunits of human ORC are dispensable for DNA replication and proliferation. *ELife*, *5*, e19084. https://doi.org/10.7554/eLife.19084.001

Wegrzyn, K., & Konieczny, I. (2023). Toward an understanding of the DNA replication initiation in bacteria. In *Frontiers in Microbiology* (Vol. 14, p. 1328842). Frontiers Media SA. https://doi.org/10.3389/fmicb.2023.1328842

Wessel, S. R., Cornilescu, C. C., Cornilescu, G., Metz, A., Leroux, M., Hu, K., Sandler, S. J., Markley, J. L., & Keck, J. L. (2016). Structure and function of the PriC DNA replication restart protein. *Journal of Biological Chemistry*, *291*(35), 18384–18396. https://doi.org/10.1074/jbc.M116.738781

Wessel, S. R., Marceau, A. H., Massoni, S. C., Zhou, R., Ha, T., Sandler, S. J., & Keck, J. L. (2013). PriC-mediated DNA replication restart requires PriC complex formation with the single-stranded DNA-binding protein. *Journal of Biological Chemistry*, *288*(24), 17569–17578. https://doi.org/10.1074/jbc.M113.478156

Windgassen, T. A., & Keck, J. L. (2016). An aromatic-rich loop couples DNA binding and ATP hydrolysis in the PriA DNA helicase. *Nucleic Acids Research*, *44*(20), 9745–9757. https://doi.org/10.1093/nar/gkw690

Windgassen, T. A., Leroux, M., Satyshur, K. A., Sandler, S. J., & Keck, J. L. (2018). Structure-specific DNA replication-fork recognition directs helicase and replication restart activities of the PriA helicase. *Proceedings of the National Academy of Sciences of the United States of America*, *115*(39), E9075–E9084. https://doi.org/10.1073/pnas.1809842115

Withers, H. L., & Bernander, R. (1998). Characterization of *dnaC2* and *dnaC28* Mutants by Flow Cytometry. *JOURNAL OF BACTERIOLOGY*, *180*(7), 1624–1631. https://journals.asm.org/journal/jb

Yoshida, R., Ozaki, S., Kawakami, H., & Katayama, T. (2023). Single-stranded DNA recruitment mechanism in replication origin unwinding by DnaA initiator protein and HU, an evolutionary ubiquitous nucleoid protein. *Nucleic Acids Research*, *51*(12), 6286–6306. https://doi.org/10.1093/nar/gkad389

Zawilak-Pawlik, A., Donczew, R., Szafrański, S., MacKiewicz, P., Terradot, L., & Zakrzewska-Czerwińska, J. (2011). DiaA/HobA and DnaA: A pair of proteins co-evolved to cooperate during bacterial orisome assembly. *Journal of Molecular Biology*, *408*(2), 238–251. https://doi.org/10.1016/j.jmb.2011.02.045

771 **Figure legend**

772 **Figure 1 Schematic structures of *oriC* and DnaA and the replication initiation mechanism.**

773 (A) Overall structure of *oriC* with the AT-rich cluster. *oriC* (245 bp) includes the Duplex-Unwinding
774 Element (DUE, purple bar) and the DnaA-Oligomerization Region (DOR, gray bar). DUE is composed
775 of three AT-rich 13-mer repeats termed L, M, and R. Dark purple boxes indicate the specific sequences
776 involved in DnaA-ssDNA binding (TT[A/G]T(T)). The AT-cluster (purple dots) flanking the DUE
777 outside *oriC* is a supplementary unwinding region. The DOR contains 12 DnaA boxes (filled and open
778 arrowheads representing sites with the full consensus TTA[A/T]NCACA sequence and sites with
779 mismatches, respectively) and an IHF-binding region (IBR, green box). The DOR is subdivided into
780 Left, Middle, and Right subregions. (B) Domains of DnaA. Domains I-IV are shown schematically,
781 with amino acid residue numbers shown in each bracket. H/B motifs (V211 and R245, squares) and
782 Arginine finger (R285, triangle) are indicated. The major functions of each domain are described on the
783 right side of the structure. (C) DUE unwinding by the ssDUE recruitment mechanism. DnaA and IHF
784 are indicated by red and green diagrams, respectively. When ATP-DnaA oligomerizes, DUE is unwound
785 unstably by thermal motion and torsional stress. The M/R region of the DUE-upper strand (purple line)
786 binds to R1-DnaA and R5M-DnaA via IHF-induced DNA bending, resulting in stable DUE unwinding.
787 In addition to M/R-DUE, L-DUE is moderately unwound and interacts with the Right-DnaA
788 subcomplex. (D) Mechanism for DnaB loading. Each Left-DnaA and Right-DnaA subcomplex binds to
789 a DnaB hexamer (blue ovals) complexed with DnaC (yellow circles). (E) PriC-dependent fork rescue
790 pathways. PriC (vivid red circle) promotes DnaB reloading to the abandoned fork, which exposes
791 ssDNA regions. PriC binds to ssDNA at the replication fork, which remodels the SSB-ssDNA complex
792 (for simplicity, SSB is omitted) for DnaC-dependent reloading of DnaB (*upper panel*). If the ssDNA
793 region is accompanied with a nascent lagging strand, Rep helicase (green shape) is recruited by PriC
794 and unwinds the lagging strand to expose the ssDNA region for DnaB loading (the lower case).

795

796 **Figure 2. Requirement of *priC* for DNA replication initiation in *dnaA46* and *dnaC2* strains.**

797 (A) Colony forming abilities. MG1655 and its derivatives MIT125 (MG1655 *dnaA46 tnaA*::Tn*10*),
798 KYA018 (MG1655 *dnaC2 zjj18*::*cat*), KRC002 (MG1655 Δ*priC*::*frt-kan*), KRC004 (MG1655 *dnaA46*
799 *tnaA*::Tn*10* Δ*priC*::*frt-kan*), and KRC005 (MG1655 *dnaC2 zjj18*::*cat* Δ*priC*::*frt-kan*) were grown
800 overnight. 10-fold-serial dilutions of the overnight cultures (~10^9 cells/mL) were incubated for 16 h at
801 30°C, or for 14 h at 35/37/42°C on LB agar medium. Three independent experiments were performed. +,
802 WT *priC*; –, Δ*priC*::*frt-kan*. The images of representative plates are shown.

803 (B) DNA replication initiation in synchronized *dnaA46* cells with or without WT *priC*. Exponentially
804 growing MIT125 (MG1655 *dnaA46 tnaA*::Tn*10*) (+) and KRC004 (MG1655 *dnaA46 tnaA*::Tn*10*

805 Δ*priC*::*frt-kan*) (–) cells were synchronized to the pre-initiation stage by incubation for 90 min at 42°C
806 in LB medium, followed by incubation for 5 min at 30°C to initiate DNA replication, which was further
807 followed by incubation with rifampicin and cephalexin for 4 h at 42°C to allow run-out of ongoing DNA
808 replication. Samples were withdrawn after synchronization and run-out replication. The DNA contents of
809 these samples were measured by flow cytometry. Representative histograms of three independent
810 experiments are shown. For each sample, the mean number of cells with more than one chromosome
811 equivalent after a 5 min release was quantified and is shown as a percentage with standard deviations.
812 (C) DNA replication initiation in synchronized *dnaC2* cells with or without WT *priC*. Exponentially
813 growing KYA018 (MG1655 *dnaC2 zjj18*::*cat*) (+) and KRC005 (MG1655 *dnaC2 zjj18*::*ca* Δ*priC*::*frt-*
814 *kan*) (–) cells were synchronized to the pre-initiation stage by incubation for 80 min at 37°C in LB
815 medium, followed by incubation for 5 min at 30°C and further incubation with rifampicin and cephalexin
816 as described above. Samples were withdrawn and analyzed as described above.
817
818 **Figure 3. Role of PriC in growth of DnaA mutant defective in interactions with DnaB.**
819 Colony forming abilities of MIT125 (MG1655 *dnaA46 tnaA*::Tn*10*) and KRC004 (MG1655 *dnaA46*
820 *tnaA*::Tn*10* Δ*priC*::*frt-kan*) cells bearing pING1 plasmid vector (–) or its derivatives pKA234 expressing
821 WT DnaA (WT) or pFH expressing DnaA F46A H136A (F46A H136A). Cells were grown at 30°C
822 overnight and 10-fold-serial dilutions of the cultures (~10^9 cells/mL) were incubated on LB agar plates
823 containing ampicillin for 16 h at 30°C and for 14 h at 42°C, respectively. Four independent experiments
824 were performed. +, WT *priC*; –, Δ*priC*::*frt-kan*.
825
826 **Figure 4. PriC stimulation of DNA replication initiation inhibited by DiaA oversupply.**
827 (A) Colony forming abilities of MG1655, KRC002 (MG1655 Δ*priC*::*frt-kan*), and FF001 (MG1655
828 Δ*rep*::*frt-kan*) cells bearing pBR322 or pNA135 (pBR322 derivatives carrying *diaA*). Overnight cultures
829 (~10^9 cells/mL) of MG1655 and KRC002 cells bearing pBR322 or pNA135 were 10-fold serially diluted
830 and incubated on LB agar plates containing ampicillin for 40 h at 25°C. The results of three independent
831 experiments were consistent, and one which is shown.
832 (B) Flow cytometry analyses of MG1655 and KRC002 (MG1655 Δ*priC*::*frt-kan*) cells bearing pBR322
833 or pNA135. Cells were exponentially grown at 30°C in LB medium with ampicillin, followed by further
834 incubation with rifampicin and cephalexin to allow run-out of chromosomal DNA replication. DNA
835 contents were quantified by flow cytometry, and cell size (mass) at the time of drug addition was
836 measured by a Coulter counter. Mean mass, ori/mass ratio, doubling time (Td), and asynchrony index
837 (A.I.: the percentage of cell numbers with non-2^n copies of *oriC* per the cell numbers with 2^n copies of
838 *oriC*) of each strain are indicated at the top right of each panel with standard deviations. Three to four

839 independent experiments were performed. +, WT *priC*; –, Δ*priC*::*frt-kan*.
840 (C) Flow cytometry analyses of MG1655, KRC003 (MG1655 Δ*priC*::*frt*), SA103 (MG1655 Δ*diaA*::*frt-*
841 *kan*), and KRC006 (MG1655 Δ*priC*::*frt*, Δ*diaA*::*frt-kan*) cells. Cells were grown and analyzed as
842 described above. Three independent experiments were performed. For "*priC*" column, +, WT *priC*;
843 –, Δ*priC*::*frt.* For "*diaA*" column, +, WT *diaA*; –, Δ*diaA*::*frt-kan.*
844
845 **Figure 5. Stimulation of replication initiation by PriC in Right-DnaA subcomplex-defective cells**
846 (A) Schematic structure of Left-*oriC* and R4*Tma oriC.* AT-rich region, DUE, and DOR are indicated by
847 a gray dotted box, a gray box, and an open box, respectively. Filled and open arrowheads in the DOR
848 show DnaA boxes with the full consensus sequence or mismatches. In addition, a striped box indicates
849 the IBR. The regions of each mutant *oriC* are indicated below the structure as open boxes. The position
850 of the *Tma*DnaA box substitution is indicated by a yellow arrowhead.
851 (B) Colony forming abilities of WT *oriC* and Left-*oriC* cells with or without WT *priC*. Overnight cultures
852 (~10^9 cells/mL) of NY20-frt (WT *oriC*; WT) and NY20L-frt (Left-*oriC*; Left) cells with (+) or without
853 (–) WT *priC* were 10-fold serially diluted and incubated on LB agar plates for 24 h at 25°C, for 16 h at
854 30°C, and for 14 h at 37°C. +, WT *priC*; –, Δ*priC*::*frt-kan*. Three independent experiments were
855 performed.
856 (C) Colony forming abilities of WT *oriC* and *oriC* R4-box mutant cells with or without WT *priC*. NY20-
857 frt (WT *oriC*) and NY24-frt (*oriC* with R4*Tma* substitution, R4*Tma*) cells with (+) or without (–) WT
858 *priC* were grown as described in panel A. +, WT *priC*; –, Δ*priC*::*frt-kan*. Four independent experiments
859 were performed.
860 (D) Flow cytometry analyses of WT and R4*Tma* cells with or without WT *priC*. Cells were exponentially
861 grown at 30°C in LB medium with ampicillin and analyzed as described in Figure 4. Representative
862 histograms from four independent experiments are shown. Mean mass, ori/mass, and Td of each strain
863 are indicated at the top right of each panel with standard deviations.
864
865 **Figure 6. Stimulation of replication initiation by PriC in cells with a deletion in the ssDNA-**
866 **expanding region of *oriC***
867 (A) Schematic structure of subATL *oriC* as shown in Figure 5. The *oriC* region including the subATL
868 *oriC* is indicated below the structure as a white box.
869 (B) Colony forming abilities of WT *oriC* and *oriC* subATL mutant cells with or without WT *priC*. NY20-
870 frt (WT *oriC*) and NY20ATL-frt (*oriC* lacking AT and L sequences, subATL) with (+) or without (–) WT
871 *priC* were grown as described in Figure 5. +, WT *priC*; –, Δ*priC*::*frt-kan.* Three independent experiments
872 were performed.

873 (C) Flow cytometry analyses of WT *oriC* and *oriC* subATL mutant cells with or without WT *priC*. Cells
874 were exponentially grown at 30°C in LB medium and analyzed as described in Figure 4. Representative
875 histograms from three independent experiments are shown. Mean mass, ori/mass, and Td of each strain
876 are indicated at the top right of each panel with standard deviations.
877
878 **Figure 7. DnaB loading onto the ssDUE by PriC.**
879 (A and B) *In vitro* reconstituted system for DnaB loading. Form I of *oriC* plasmid (pBS*oriC*; 1.6 nM) was
880 incubated for 15 min at 30°C with the indicated amount of PriC in the presence of ATP-DnaA or its mutant
881 derivatives, DnaB, DnaC, IHF, gyrase, and SSB. The resulting plasmids were purified and analyzed using
882 agarose gel electrophoresis. A representative image of three independent experiments is shown in the
883 black/white-inverted mode (A). Band intensities of each lane in the gel image were analyzed by
884 densitometric scanning. The percentages of form I* *oriC* plasmid per input DNA are shown as 'Form I*
885 (%)'. Mean and standard deviations are shown (B). Abbreviations in panel B: –, no addition of DnaA;
886 WT, wild-type DnaA; FH, DnaA F46A H136A; VA, DnaA V211A.
887 (C and D) *In vitro* reconstituted system containing DiaA. Form I of pBS*oriC* plasmid was used as
888 described above except for the addition of the indicated amounts of DiaA. A representative image of three
889 independent experiments is shown in black/white-inverted mode (C). Band intensities of each lane in the
890 gel image were analyzed by densitometric scanning. The percentages of form I**oriC* plasmid together
891 with the mean and standard deviations are shown as described above (D).
892
893 **Figure 8. PriC stimulation of cSDR-dependent cell growth.**
894 (A) Colony forming abilities. Cells of MIT125 (MG1655 *dnaA46*), MIT125c (MG1655 *dnaA46*
895 *rnhA*::*cat*), KRC004 (MG1655 *dnaA46* Δ*priC*::*frt-kan*), and KRC004c (MG1655 *dnaA46* Δ*priC*::*frt-kan*
896 *rnhA*::*cat*) were grown at 30°C overnight and 10-fold-serial dilutions of the overnight cultures (~10^9
897 cells/mL) were incubated for 16 h at 30°C and for 36 h at 40°C on LB agar plates. Three independent
898 experiments were performed. +, WT; –, deletion.
899 (B) *oriC* and *ter* copy numbers. MIT125, MIT125c, KRC004, and KRC004c cells growing exponentially
900 at 30°C were further incubated for 90 min at 40°C in LB medium. Samples were withdrawn before and
901 after the 40°C incubation. The genome DNA of each sample was extracted by boiling the cells for 5 min
902 at 95°C. The relative copy numbers of *oriC* (84.6 min) and *ter* (32.4 min) to that of *yapB* (50.5 min) were
903 quantified using real-time qPCR. The data and averages of three independent experiments are shown with
904 standard deviations.
905
906 **Figure 9. Model for PriC-promoted replication initiation.**

907 PriC-promoted rescue of blocked DnaA-*oriC* dependent replication initiation. *oriC*, DnaA, IHF, DnaB,
908 and DnaC are illustrated as depicted in Figure 1C. When tight DnaA binding of DiaA (dark gray circle)
909 (or DnaA F46A H136A double mutations) inhibits DnaB recruitment, PriC (Brilliant red circle) binds to
910 a stably unwound DUE strand, recruiting a DnaB-DnaC complex to lower strand of DUE instead of
911 Left-DnaA subcomplex. When a sufficient ssDNA region is exposed, PriC then recruits the DnaB-DnaC
912 complex to the opposite strand.
913
914
915 **Figure 4-figure supplement 1. Colony formation of cells carrying pBR322 or pNA135 with WT *priC***
916 **or Δ*priC*::*frt-kan*.**
917 Colony forming abilities of MG1655 or KRC002 (MG1655 Δ*priC*::*frt-kan*) cells bearing pBR322 or
918 pNA135 (pBR322 derivatives carrying *diaA*). Overnight cultures (~10^9 cells/mL) of MG1655 and
919 KRC002 cells carrying pBR322 or pNA135 were 10-fold serially diluted and incubated on LB agar plates
920 containing ampicillin for 14 h at 30–42°C. +, WT *priC*; –, Δ*priC*::*frt-kan*. The results of three independent
921 experiments were consistent, and one representative result is shown.
922
923 **Figure 7-figure supplement 1. DUE unwinding activities of DnaA mutant deriviatives in the**
924 **presence and absence of PriC.**
925 (A and B) *in vitro* DUE unwinding assays using DnaA mutant derivatives. Form I of *oriC* (pBS*oriC*; 1.6
926 nM) was incubated for 9 min at 30°C with the indicated amount of DnaA or its mutant derivatives in the
927 presence of IHF (42 nM), followed by incubation with P1 nuclease (1.5 units) and further incubation with
928 AlwNI before agarose gel electrophoresis. Note that 2.6 kb and 1.0 kb fragments are observed with
929 restriction enzyme digestion when the ssDNA-specific P1 nuclease cleaves 3.6 kb pBS*oriC* at the DUE.
930 A representative image of two independent experiments is shown in black/white-inverted mode (A). The
931 sizes of each band are indicated at the left side of the image. Bands intensities of each lane in the gel
932 image were analyzed by densitometric scanning. The percentages of P1 nuclease-digested *oriC* DNA per
933 input DNA molecules are shown as 'DUE unwinding (%)'. Mean and data are shown (B). Abbreviations
934 in panel B: –, no addition of DnaA; WT, wild-type DnaA; FH, DnaA F46A H136A; VA, DnaA V211A.
935 (C and D) *In vitro* DUE unwinding assay with PriC. pBS*oriC* was used as described above except for
936 PriC addition. A representative image of two independent experiments is shown in black/white-inverted
937 mode (C). Data were analyzed as described above (D). n.t., not tested.

Key Resources Table				
Reagent type (species) or resource	**Designation**	**Source or reference**	**Identifiers**	**Additional information**
strain, strain background (*Escherichia coli*)	BW25113 Δ*priC*::*frt-kan*	Keio collection	JW0456-KC	
strain, strain background (*Escherichia coli*)	BW25113 Δ*rep*::*frt-kan*	Keio collection	JW5604-KC	
strain, strain background (*Escherichia coli*)	MG1655 *dnaC2 zjj18*::*cat*	Kasho and Katayama, 2013	KYA018	
strain, strain background (*Escherichia coli*)	MG1655 *dnaA46 tnaA*::Tn10	Noguchi, *et al.*, 2016	MIT125	
strain, strain background (*Escherichia coli*)	MG1655 *rnhA*::*cat*	Noguchi, *et al.*, 2016	MIT162	
strain, strain background (*Escherichia coli*)	MG1655 Δ*diaA*::*frt-kan*	Noguchi, *et al.*, 2016	SA103	
strain, strain background (*Escherichia coli*)	MG1655 Δ*priC*::*frt-kan*	This work	KRC002	MG1655 x P1 JW0456-KC
strain, strain background (*Escherichia coli*)	MG1655 Δ*priC*::*frt*	This work	KRC003	KRC002 x pCP20

strain, strain background (*Escherichia coli*)	MIT125 Δ*priC*::*frt-kan*	This work	KRC004	MIT125 x P1 JW0456-KC
strain, strain background (*Escherichia coli*)	KYA018 Δ*priC*::*frt-kan*	This work	KRC005	KYA018 x P1 JW0456-KC
strain, strain background (*Escherichia coli*)	KRC003 Δ*diaA*::*frt-kan*	This work	KRC006	KRC003 x P1 SA103
strain, strain background (*Escherichia coli*)	MG1655 Δ*rep*::*frt-kan*	This work	FF001	MG1655 x P1 JW5604-KC
strain, strain background (*Escherichia coli*)	MG1655 *asnA*::*frt-kan*	Noguchi, *et al*, 2015	NY20	
strain, strain background (*Escherichia coli*)	MG1655 *asnA*::*frt-kan* *oriC*ΔR4 box::*Tma*DnaA box	Noguchi, *et al*, 2015	NY21	
strain, strain background (*Escherichia coli*)	MG1655 *asnA*::*frt-kan* *oriC*ΔMiddle-Right DOR	This work	NY20L	
strain, strain background (*Escherichia coli*)	MG1655 *asnA*::*frt-kan* *oriC*ΔAT-L region	This work	NY20ATL	

strain, strain background (*Escherichia coli*)	MG1655 *asnA*::*frt*	Yoshida, *et al*, 2023	NY20-frt	
strain, strain background (*Escherichia coli*)	MG1655 *asnA*::*frt* *oriC*ΔR4 box::*Tma*DnaA box	This work	NY21-frt	NY21 x pCP20
strain, strain background (*Escherichia coli*)	MG1655 *asnA*::*frt* *oriC*ΔMiddle-Right DOR	This work	NY20L-frt	NY20L x pCP20
strain, strain background (*Escherichia coli*)	MG1655 *asnA*::*frt* *oriC*ΔAT-L region	This work	NY20ATL -frt	NY20ATL x pCP20
strain, strain background (*Escherichia coli*)	NY20-*frt* Δ*priC*::*frt-kan*	This work	NY20-*priC*	NY20-frt x P1 KRC002
strain, strain background (*Escherichia coli*)	NY21-*frt* Δ*priC*::*frt-kan*	This work	NY21-*priC*	NY21-frt x P1 KRC002
strain, strain background (*Escherichia coli*)	NY20L-*frt* Δ*priC*::*frt-kan*	This work	NY20L-*priC*	NY20L-frt x P1 KRC002
strain, strain background (*Escherichia coli*)	NY20ATL-*frt* Δ*priC*::*frt-kan*	This work	NY20ATL -*priC*	NY20ATL-frt x P1 KRC002

strain, strain background (*Escherichia coli*)	MIT125 Δ*rnhA*::*cat*	This work	MIT125c	MIT125 x P1 MIT162
strain, strain background (*Escherichia coli*)	KRC004 Δ*rnhA*::*cat*	This work	KRC004c	KRC004 x P1 MIT162
Recombinant DNA reagent	pING1 (Plasmid)	Katayama, *et al.*, 1994		Vector bearing arabinose-inducible promoter
Recombinant DNA reagent	pKA234 (Plasmid)	Kubota, *et al.,* 1997		pING1 encoding *dnaA*
Recombinant DNA reagent	pH136A (Plasmid)	Sakiyama, *et al.*, 2018		pKA234 *dnaA* H136A
Recombinant DNA reagent	pFH (Plasmid)	This study		pH136A mutated by Quick Change site-directed mutagenesis by primers F46A 1/2
Recombinant DNA reagent	pKW44-1 (Plasmid)	Ozaki, *et al.,* 2008		pKA234 *dnaA* V211A
Recombinant DNA reagent	pNA135 (Plasmid)	Ishida, *et al.*, 2004		pBR322 bearing *diaA* gene
Recombinant DNA reagent	pBS*oriC* (Plasmid)	Kawakami , *et al.* 2005		pBluescript bearing a 678 bp chromosome-derived region including *oriC*
Recombinant DNA reagent	pET22b(+)-priC (Plasmid)	Aramaki, *et al.*, 2015		pET22b(+) bearing *priC* under the T7 promoter

Recombinant DNA reagent	pTKM601 (Plasmid)	Keyamura, *et al.*, 2007		pBAD/HisB bearing *diaA*
Sequence-based reagent	F46A 1	Keyamura *et al.*, 2009	PCR primer	GTACGCGCCAAACCGCGCGGTCCTTCGATTGGGTACG
Sequence-based reagent	F46A 2	Keyamura *et al.*, 2009	PCR primer	CGTACCCAATCGAAGGACCGCGCGGTTTGGCGCGTAC
Sequence-based reagent	ORI_1	Kasho *et al.*, 2014	qPCR primer	CTGTGAATGATCGGTGATC
Sequence-based reagent	KW*oriC*Rev	Kasho *et al.*, 2014	qPCR primer	GTGGATAACTCTGTCAGGAAGCTTG
Sequence-based reagent	qoriK fw	Brochu *et al.*, 2014	qPCR primer	CGAGACTTCAGCGACAGTTAAG
Sequence-based reagent	qoriK rev	Brochu *et al.*, 2014	qPCR primer	CCTGCGGATATTTGCGATACA
Sequence-based reagent	STM419	This work	qPCR primer	CGGACACCTTGTCTGACCTAAG
Sequence-based reagent	STM420	This work	qPCR primer	AGTGTGAAAATGACCCTCTTGC

Figure 1

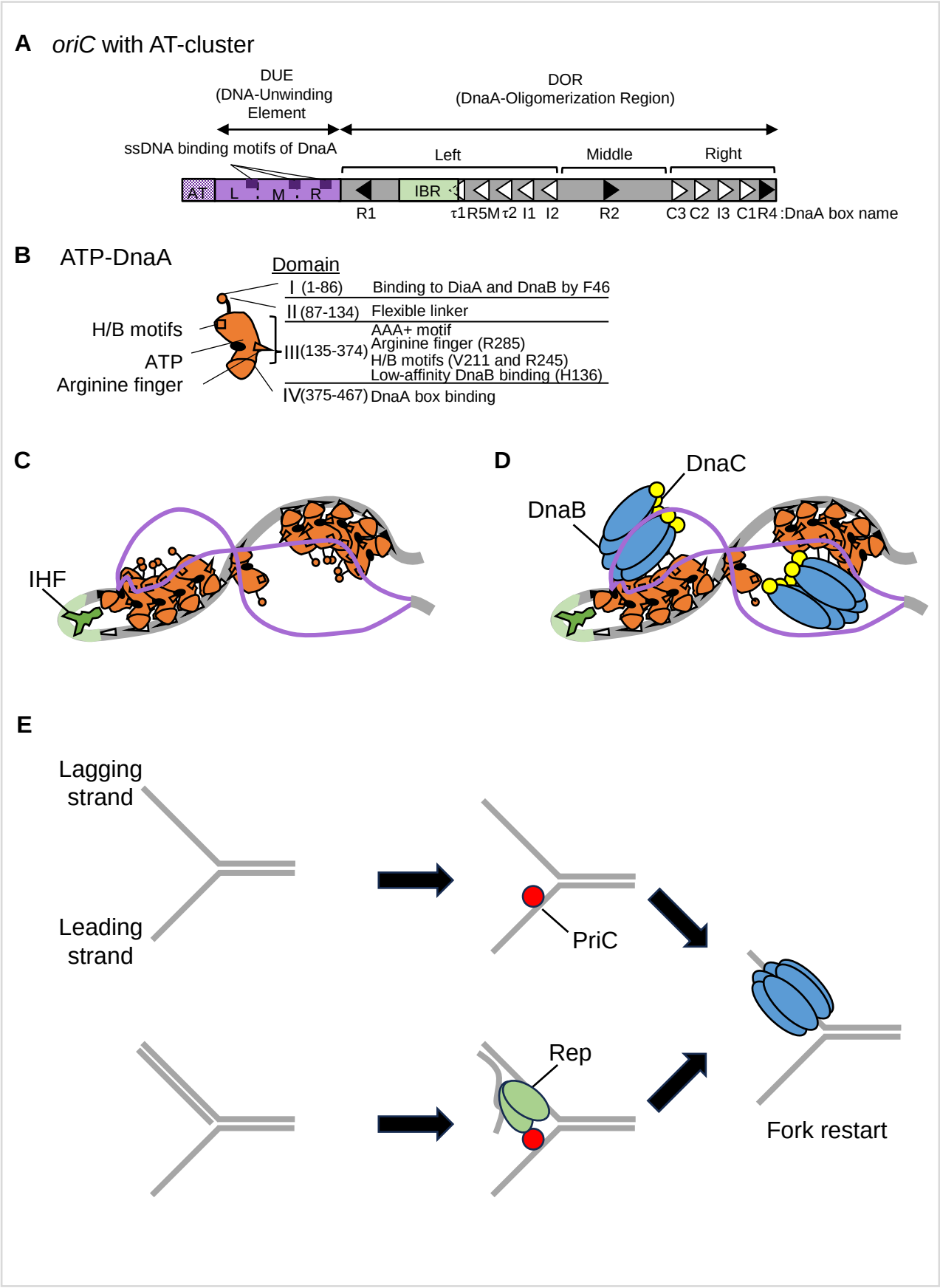
A
oriC with AT-cluster
DUE
(DNA-Unwinding
Element
DOR
(DnaA-Oligomerization Region)
ssDNA binding motifs of DnaA
Left
Middle
Right
AT
L
M
R
IBR
R1
τ1
R5M
τ2
I1
I2
R2
C3
C2
I3
C1
R4
:DnaA box name
B
ATP-DnaA
Domain
H/B motifs
ATP
Arginine finger
I (1-86)
Binding to DiaA and DnaB by F46
II (87-134)
Flexible linker
III(135-374)
AAA+ motif
Arginine finger (R285)
H/B motifs (V211 and R245)
Low-affinity DnaB binding (H136)
IV(375-467)
DnaA box binding
C
IHF
D
DnaC
DnaB
E
Lagging
strand
Leading
strand
PriC
Rep
Fork restart

Figure 2

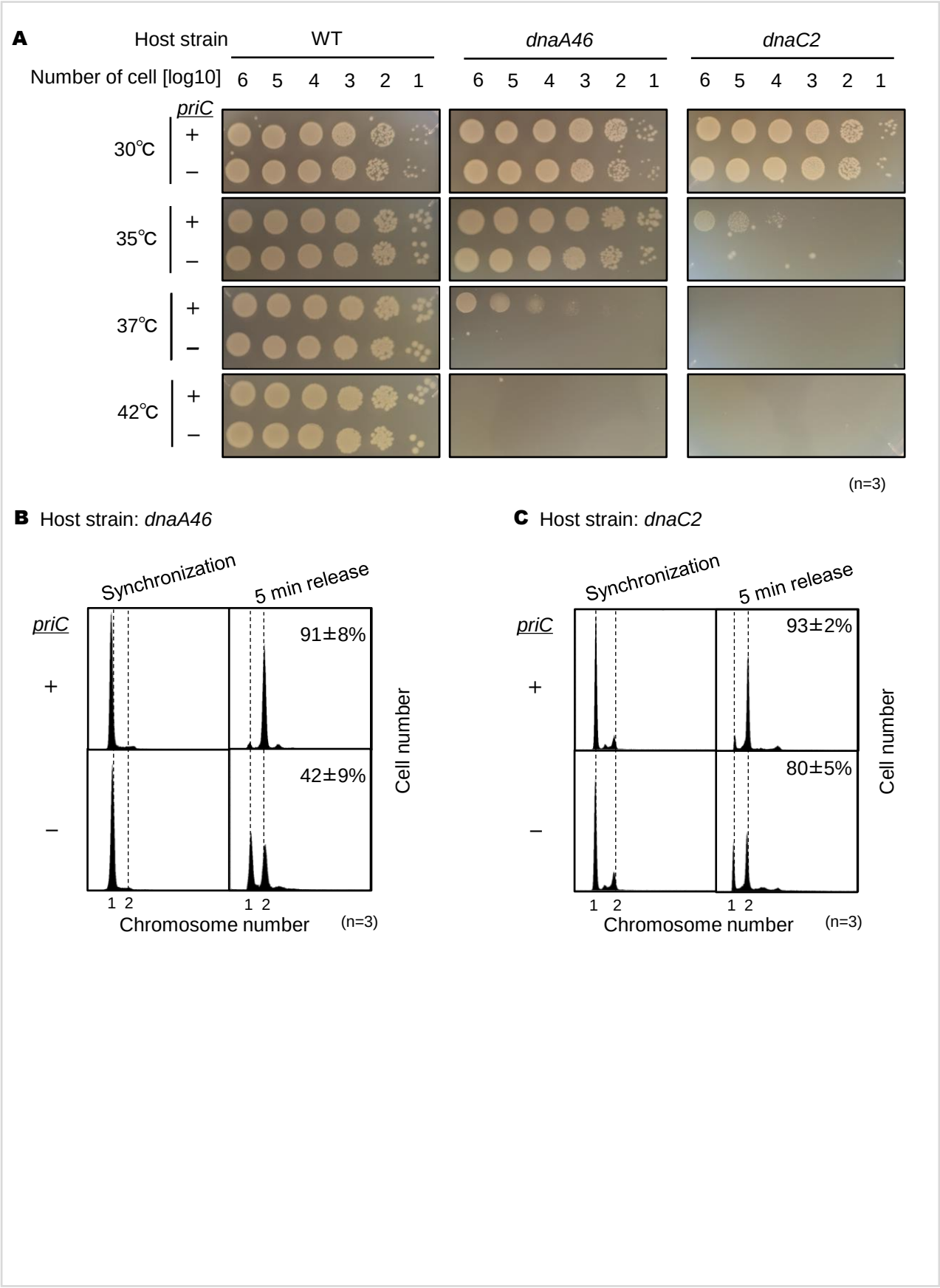
A
Host strain
WT
dnaA46
dnaC2
Number of cell [log10]
6 5 4 3 2 1
priC
30℃
35℃
37℃
42℃
+
−
(n=3)
B Host strain: dnaA46
Synchronization
5 min release
91±8%
42±9%
Cell number
1 2
Chromosome number
(n=3)
C Host strain: dnaC2
93±2%
80±5%

Figure 3

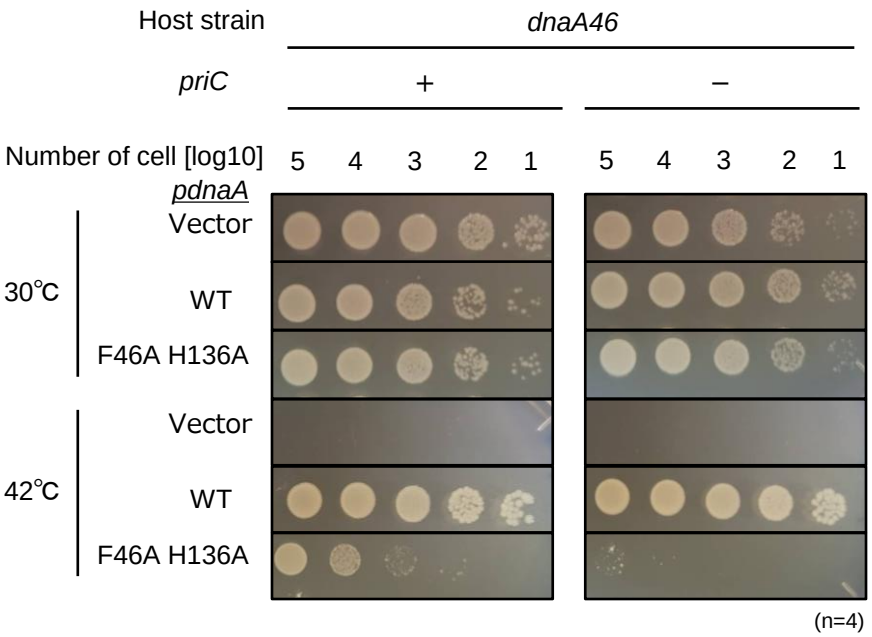
Host strain
dnaA46
priC
+
−
Number of cell [log10]
5 4 3 2 1
5 4 3 2 1
pdnaA
30℃
Vector
WT
F46A H136A
42℃
Vector
WT
F46A H136A
(n=4)

Figure 4

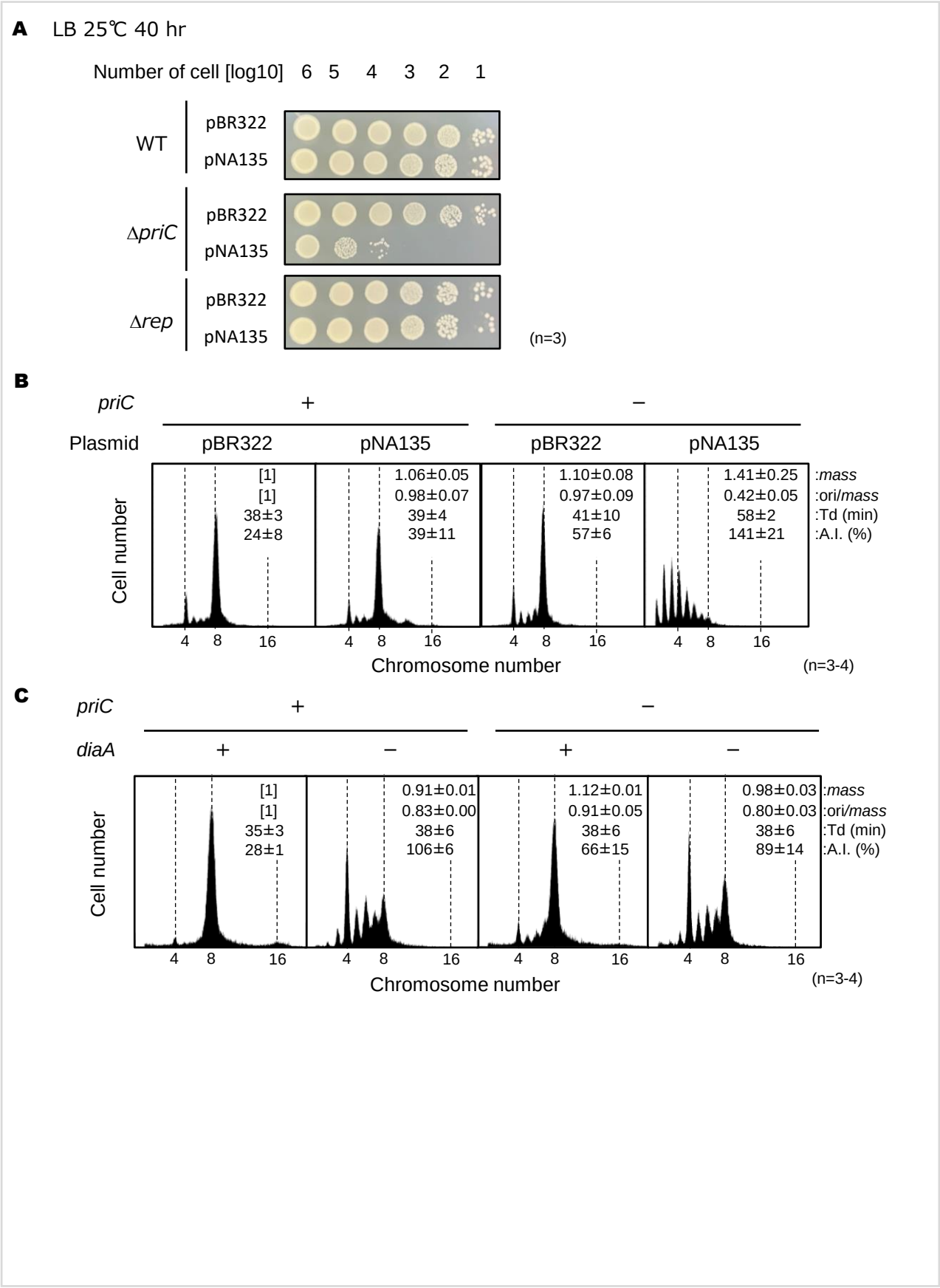
A
LB 25℃ 40 hr
Number of cell [log10] 6 5 4 3 2 1
WT
pBR322
pNA135
ΔpriC
pBR322
pNA135
Δrep
pBR322
pNA135
(n=3)
B
priC
+
−
Plasmid
pBR322
pNA135
pBR322
pNA135
[1]
[1]
38±3
24±8
1.06±0.05
0.98±0.07
39±4
39±11
1.10±0.08
0.97±0.09
41±10
57±6
1.41±0.25
0.42±0.05
58±2
141±21
:mass
:ori/mass
:Td (min)
:A.I. (%)
Cell number
4 8 16
Chromosome number
(n=3-4)
C
priC
+
−
diaA
+
−
+
−
[1]
[1]
35±3
28±1
0.91±0.01
0.83±0.00
38±6
106±6
1.12±0.01
0.91±0.05
38±6
66±15
0.98±0.03
0.80±0.03
38±6
89±14
:mass
:ori/mass
:Td (min)
:A.I. (%)
Cell number
4 8 16
Chromosome number
(n=3-4)

Figure 5

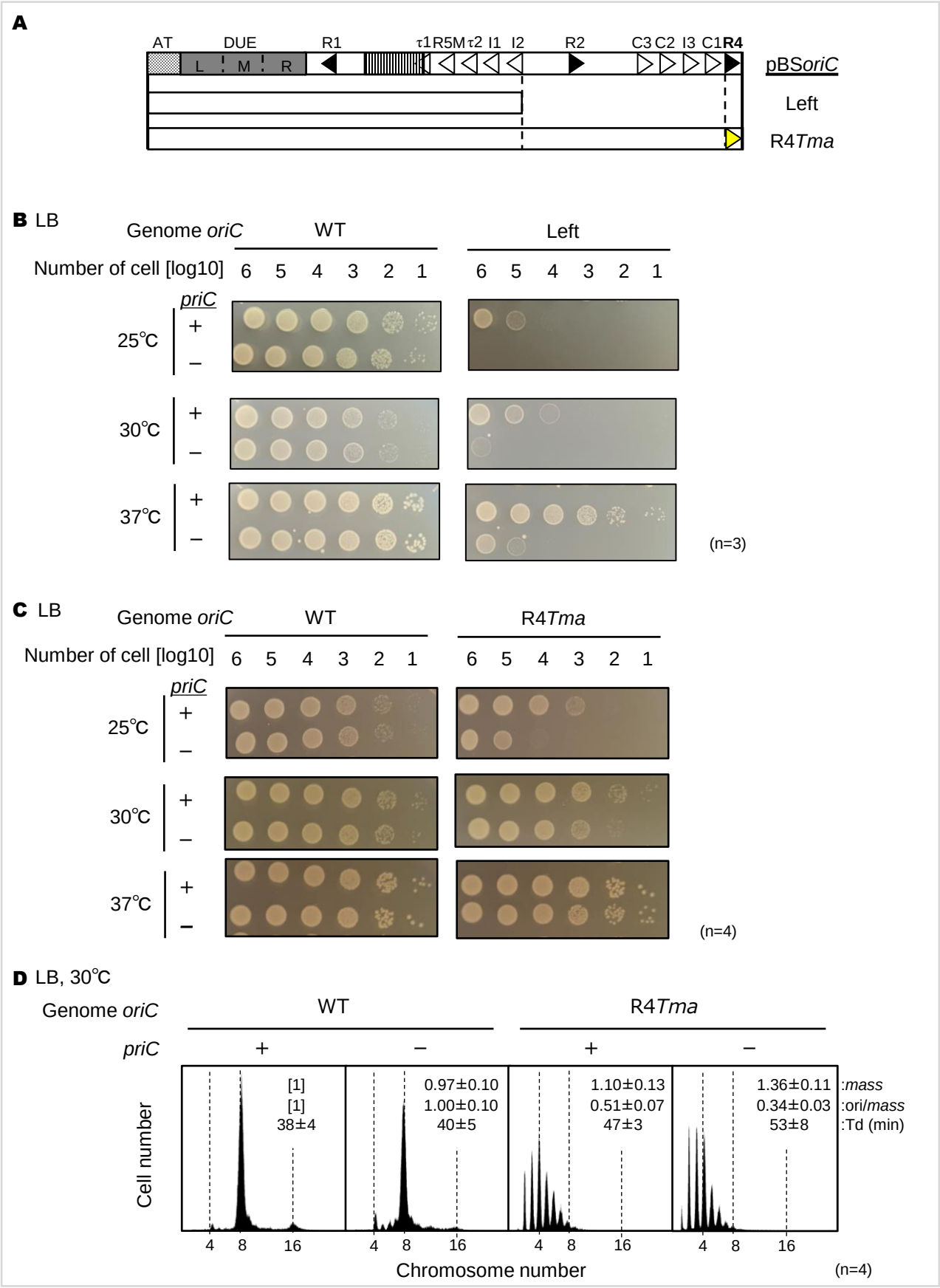
A
AT
DUE
L
M
R
R1
τ1
R5M
τ2
I1
I2
R2
C3
C2
I3
C1
R4
pBSoriC
Left
R4Tma
B LB
Genome oriC
WT
Left
Number of cell [log10]
6 5 4 3 2 1
priC
25℃
30℃
37℃
+
−
(n=3)
C LB
Genome oriC
WT
R4Tma
Number of cell [log10]
6 5 4 3 2 1
priC
25℃
30℃
37℃
+
−
(n=4)
D LB, 30℃
Genome oriC
WT
R4Tma
priC
+
−
+
−
Cell number
[1]
[1]
38±4
0.97±0.10
1.00±0.10
40±5
1.10±0.13
0.51±0.07
47±3
1.36±0.11
0.34±0.03
53±8
:mass
:ori/mass
:Td (min)
4 8 16
Chromosome number
(n=4)

Figure 6

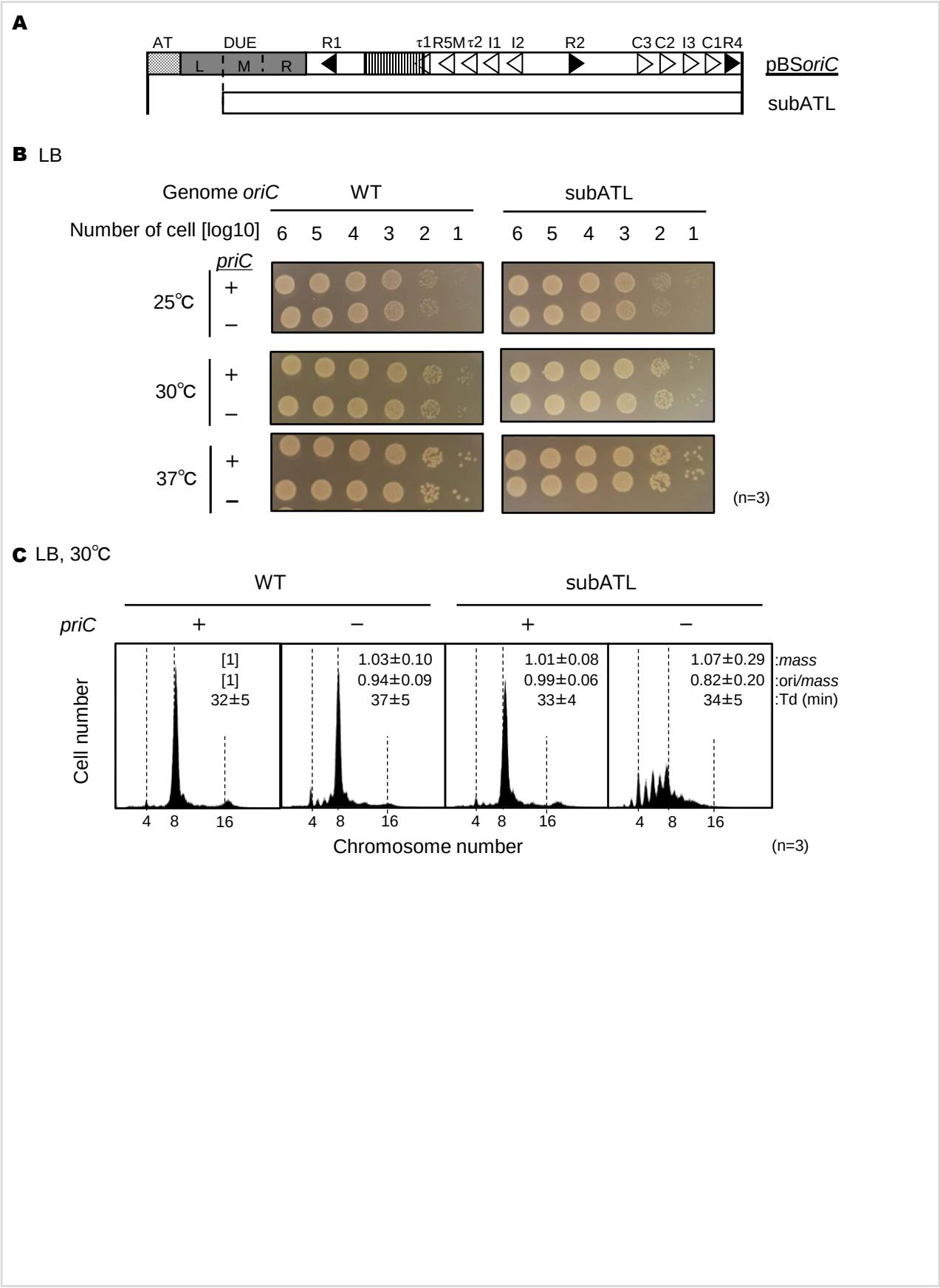
A
AT
DUE
L
M
R
R1
τ1
R5M
τ2
I1
I2
R2
C3
C2
I3
C1
R4
pBSoriC
subATL
B LB
Genome oriC
WT
subATL
Number of cell [log10]
6 5 4 3 2 1
6 5 4 3 2 1
priC
25℃
30℃
37℃
+
−
(n=3)
C LB, 30℃
WT
subATL
priC
+
−
+
−
[1]
[1]
32±5
1.03±0.10
0.94±0.09
37±5
1.01±0.08
0.99±0.06
33±4
1.07±0.29
0.82±0.20
34±5
:mass
:ori/mass
:Td (min)
Cell number
4 8 16
Chromosome number
(n=3)

Figure 7

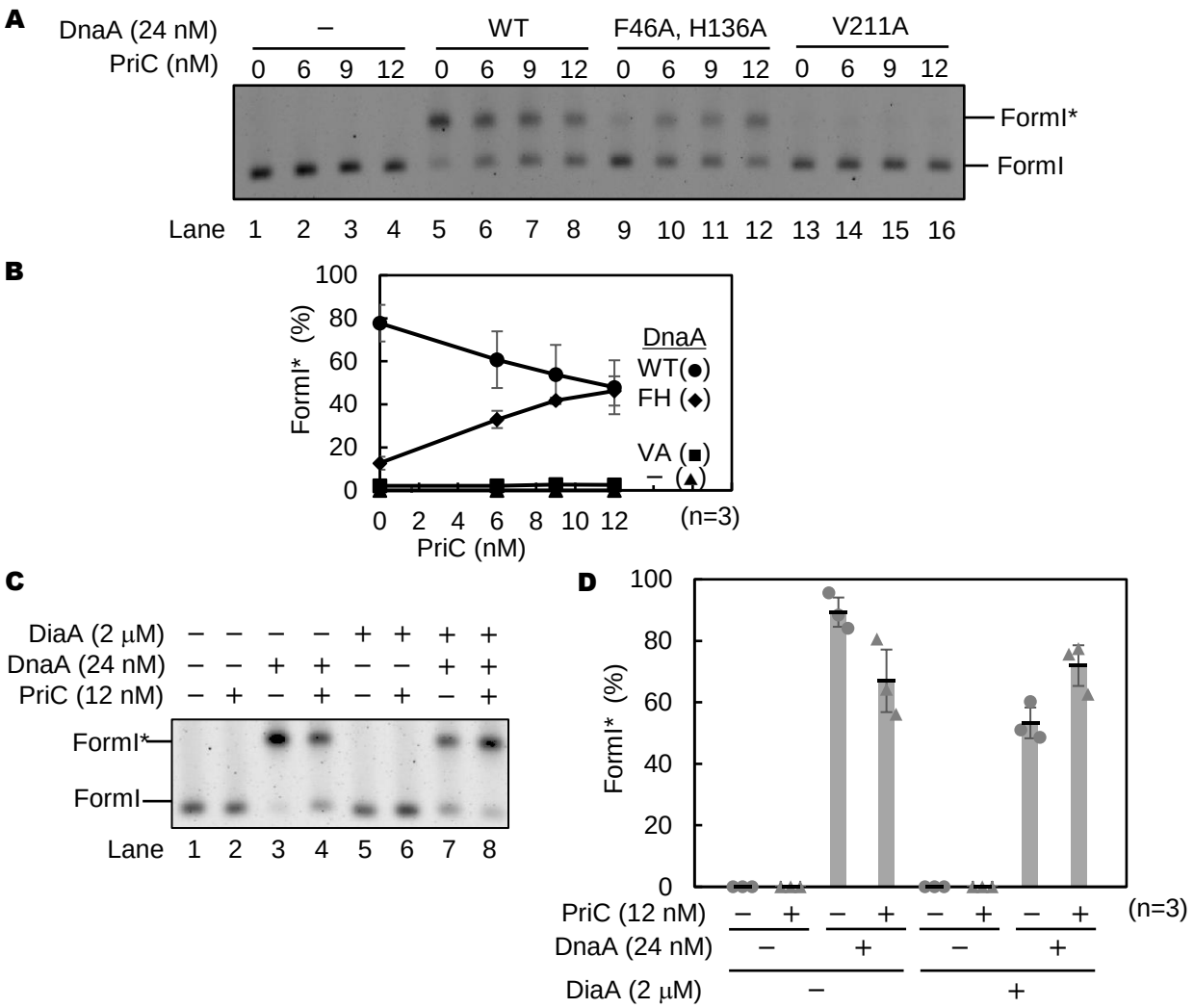
A
DnaA (24 nM)
PriC (nM)
–
WT
F46A, H136A
V211A
0 6 9 12 0 6 9 12 0 6 9 12 0 6 9 12
FormI*
FormI
Lane 1 2 3 4 5 6 7 8 9 10 11 12 13 14 15 16
B
FormI* (%)
100
80
60
40
20
0
DnaA
WT(●)
FH (◆)
VA (■)
– (▲)
0 2 4 6 8 10 12
PriC (nM)
(n=3)
C
DiaA (2 μM) – – – – + + + +
DnaA (24 nM) – – + + – – + +
PriC (12 nM) – + – + – + – +
FormI*
FormI
Lane 1 2 3 4 5 6 7 8
D
FormI* (%)
100
80
60
40
20
0
PriC (12 nM) – + – + – + – +
DnaA (24 nM) – + – +
DiaA (2 μM) – +
(n=3)

Figure 8

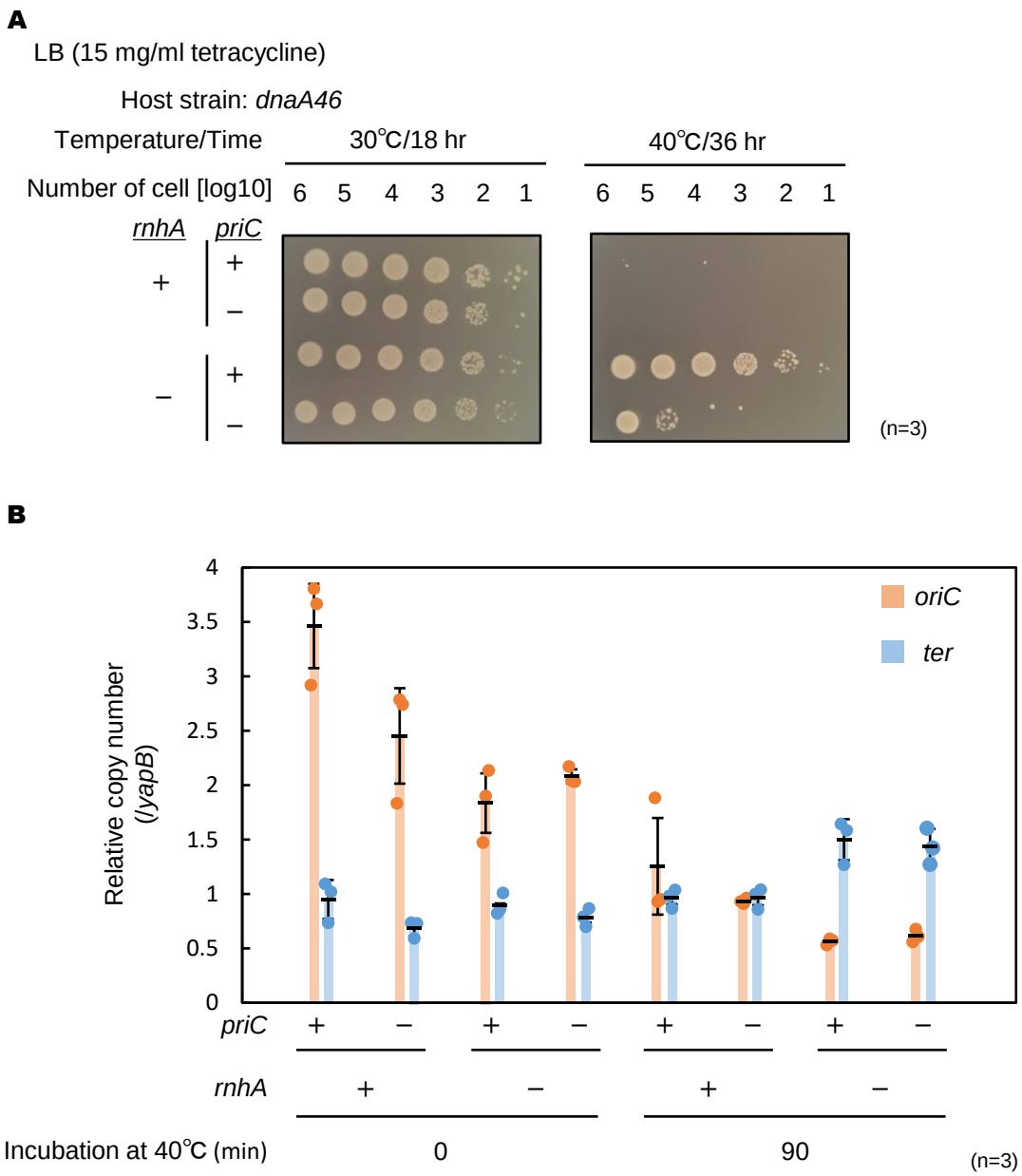
A
LB (15 mg/ml tetracycline)
Host strain: dnaA46
Temperature/Time
30℃/18 hr
40℃/36 hr
Number of cell [log10]
6 5 4 3 2 1
6 5 4 3 2 1
rnhA
priC
+
−
+
−
+
−
(n=3)
B
Relative copy number (IyapB)
4
3.5
3
2.5
2
1.5
1
0.5
0
oriC
ter
priC
+ − + − + − + −
rnhA
+ − + −
Incubation at 40℃ (min)
0
90
(n=3)

Figure 9

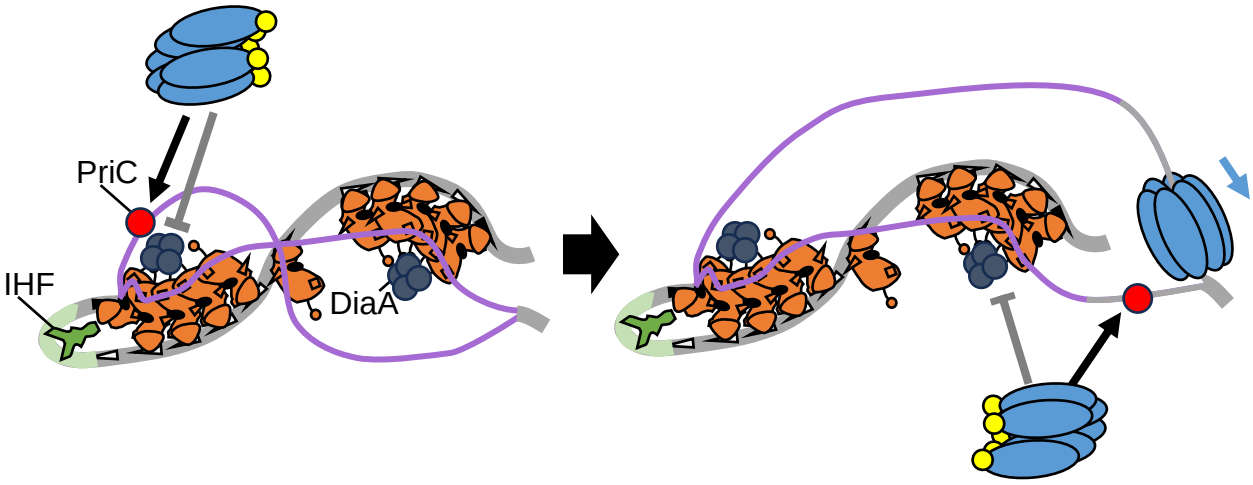

Figure 4-figure supplement 1

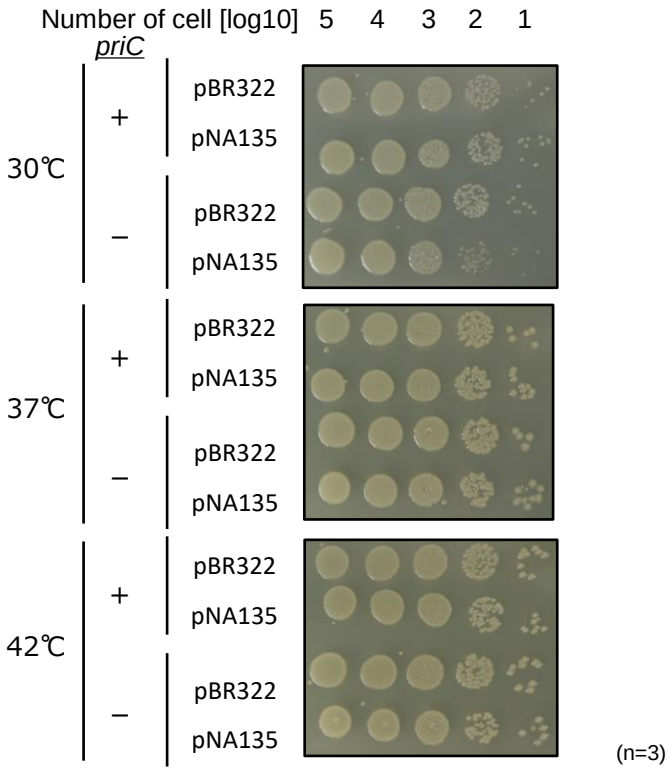

(n=3)
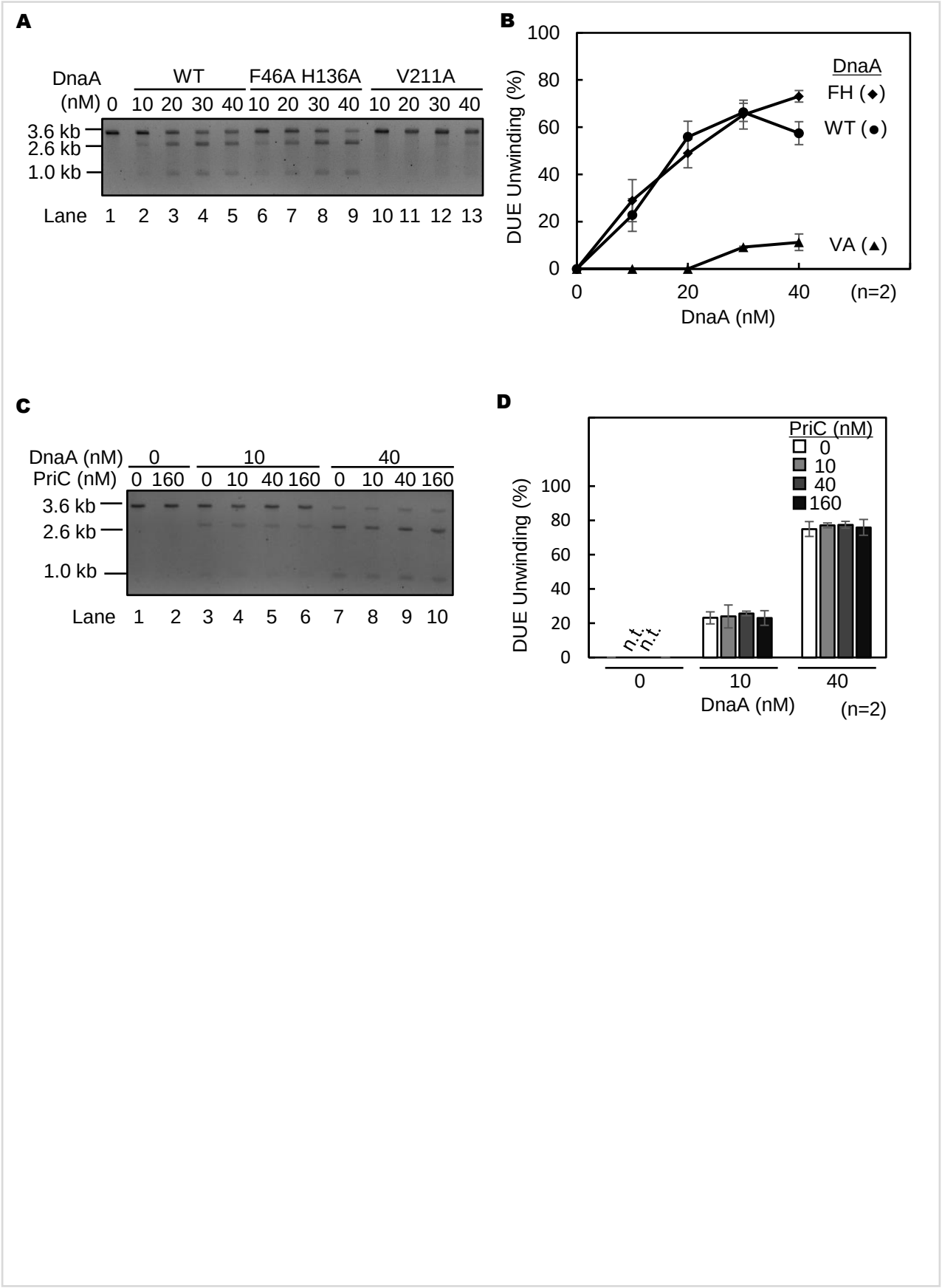
Figure 7-figure supplement 1